An analysis of the catalytic performance of supported Ni in hydrotreating

Rodrigo Valderrama Zapata

Trabajo de grado presentado como requisito para optar el título de Ingeniero Químico

Director
Víctor Gabriel Baldovino Medrano
Ingeniero Químico, PhD.

Co-directores
Iván Darío Mora Vergara
Ingeniero Químico, MSc
César Augusto Luna Cáceres
Químico, MSc

Universidad Industrial de Santander
Facultad de Ingenierías Fisicoquímicas
Escuela de Ingeniería Química
Bucaramanga
2020

Dedicatoria

"En la Esperanza del mañana está la Fortaleza del hoy"

Este logro va dedicado a mis padres ***Rosa*** *y* ***Rodrigo*** *por ser mi motor de vida, mi respaldo, mi aliento de seguir, y por ser la razón para seguir en pie día a día.*

A mis hermanas ***Keyla*** *y* ***Elizabeth,*** *por ustedes hago lo que sea.*

A ***Santiago****, mi pequeño sobrino, quien me reemplazó como el niño de la casa, sigue sonriendo como lo has hecho siempre.*

Agradecimientos

Agradezco primeramente a Dios por ser mi luz, mi guía, por haberme puesto en donde estoy ahora, por darme fuerzas cuando más las necesitaba, por nunca abandonarme y por siempre mostrarme la solución a los problemas.

A la Universidad Industrial de Santander por ser mi alma mater, por abrirme sus puertas para permitirme formar como excelente profesional y por mostrarme que sí hay formas de hacer el cambio que tanto anhelamos en el país.

A la sede UIS Barrancabermeja por recibirme los primeros años de la carrera, por ser mi puente entre el colegio y la universidad, por permitirme demostrar que la procedencia, la sede y los factores económicos no necesariamente definen a un buen estudiante.

A la Escuela de Ingeniería Química por ser mi segundo hogar en los últimos años, por mostrarme lo hermoso que es esta profesión, por permitirme conocer excelentes personas y vivir grandes momentos.

Al Centro de Investigación en Catálisis CICAT-UIS por abrirme sus puertas desde el semillero de investigación, por permitirme realizar este proyecto en sus instalaciones, por financiarlo, por ayudarme y apoyarme a formar como un buen investigador y por ser un excelente grupo en el que pude conocer grandes estudiantes colegas, profesionales y profesores.

A los grupos de investigación GIP y GIMBA por permitirme realizar los análisis necesarios para culminar mi proyecto.

A mi director, el profesor Víctor Baldovino, por orientarme, por hacerme dudar siempre y así permitir encontrar la mejor respuesta a los acontecimientos, por apoyarme, por ayudarme, por mostrarme lo hermoso que es la investigación y por mantener su confianza en mí.

A Iván Mora por guiarme y acompañarme en gran parte del desarrollo del proyecto. A Stivenson, María, Carol, Rosa, Carolina, Mery, Diana, Laura, Estefany, Mauricio, Raúl, Julieth, Paula, Henry y demás miembros del CICAT por ser excelentes personas y colegas que me dieron una mano siempre que la necesite y me acompañaron muchos momentos buenos.

Al Capítulo Estudiantil AIChE-UIS y todos sus miembros actuales y antiguos por haberme hecho ser una mejor persona al mostrarme todo lo bueno que se puede hacer cuando uno se lo propone, por haberme permitido conocer grandes personas, por haberme hecho vivir excelentes experiencias y por impulsarme a buscar lo mejor para todos y cada uno de los me acompañan.

A la profesora Diana por aconsejarme y querer que dé lo mejor de mí siempre. A los profesores Gustavo, César, Wilber, Robinson y muchos otros que me orientaron muy bien y me forjaron como un gran profesional íntegro.

A los 17 fantásticos por darme tantos momentos de risa, de comidas, por respaldarme cuando tenía mil cosas pendientes y aun así me ayudaron a responder adecuadamente, y porque me ayudaron a mostrar que se puede trabajar muy bien en equipo sin importar la procedencia.

A mis familiares Alcira, Yunny, Adalgiza, Fernando y Jeysson por haberme apoyado y ayudado de una u otra forma a conseguir completar este logro.

A mis amigos del colegio y de toda la vida Silvia, Julián y Jaime por darme voz de aliento siempre que la necesité, por estar ahí conmigo después de tanto tiempo, por ayudarme a salir de la rutina de vez en cuando, por todas las horas que hemos pasado hablando de todo y de nada y por todo el tiempo que me dedicaron cuando más ocupados estaban.

Finalmente, gracias a todas las personas que me ayudaron a cumplir con este logro tan anhelado para mí.

Contents

Figures List

Tables List

Appendix List

Abbreviations List

ASA	Amorphous Aluminosilicate
BCH	Benzylcyclohexane
BET	Brunauer - Emmett - Teller
BJH	Barrett - Joyner - Halenda
CH	Cyclohexane
CHB	Cyclohexylbenzene
CP	Cracking Products
CTAB	Cetyl Trimethyl Ammonium Bromide
DBT	Dibenzothiophene
DDS	Direct Desulfurization
DMDBT	Dimethyl-DBT
EB	Ethylbenzene
ECH	Ethylcyclohexane
ECHE	Ethylcyclohexene
GC	Gas Chromatography
GC-MS	GC - Mass Spectroscopy
HDA	Hydrodearomatization
HDM	Hydrodemetallization
HDN	Hydrodenitrogenation
HDS	Hydrodesulfurization
HDT	Hydrotreating
HHDBT	Hexahydro-DBT
HIN	Indoline
HYD	Hydrogenation
IND	Indole
NLDFT	Non-Local Density Functional Theory
OEA	Orthoethylalinine
OECHA	Ethylcyclohexylamine
OHI	Octahydroinoline
PAD	Proton Affinity Distribution
PS	Size Pore
PZC	Point of Zero Charge
SA	Specific Area
SEA	Strong Electrostatic Adsorption
TGA	Thermogravimetry Analysis
THDBT	Tetrahydro-DBT
VP	Volume Pore

Resumen

Título: Análisis del desempeño catalítico en hidrotratamiento de Ni soportado[†].

Autor: Rodrigo Valderrama Zapata[‡].

Palabras Clave: níquel metálico, hidrotratamiento, hidrodesulfuración, zeolita jerárquica, adsorción electrostática fuerte.

Descripción:

El consumo de combustibles a nivel mundial sigue en aumento. La combustión de estos puede generar compuestos gaseosos como los óxidos de azufre (SO_x) que son altamente contaminantes para el medio ambiente y perjudiciales para la salud. Para tratar de mitigar este impacto negativo, se opta por realizar procesos como el hidrotratamiento (HDT), con el fin de remover la mayor cantidad de moléculas que puedan contribuir a estas afectaciones. El fin de este trabajo se centra en explorar el comportamiento catalítico en reacciones de hidrotratamiento de Ni soportado en varios aluminosilicatos, especialmente sobre una zeolita jerárquica tipo Y. Para esto, se utilizaron 4 soportes: una sílice de baja área superficial, una alúmina comercial, una zeolita tipo Y comercial, y esta misma, pero se modificó su estructura a fin de generar la existencia de microporos y mesoporos simultáneamente. A estos soportes se les impregnó Ni mediante el método de adsorción electrostática fuerte (SEA, por sus siglas en inglés). Se evaluaron las propiedades fisicoquímicas tanto de los soportes como de los catalizadores y finalmente se probaron en reacciones de hidrodesulfuración (HDS) de dibenzotiofeno (DBT) con y sin la presencia de indol como compuesto nitrogenado. Los resultados mostraron que el uso de la zeolita micro-mesoporosa como soporte, llevó a los resultados de actividad más altos, mientras que con la sílice y la alúmina la conversión se hace prácticamente cero a partir de la segunda hora de reacción. También se observó que la presencia de un compuesto nitrogenado promueve la HDS del DBT, aumentando la conversión por un factor aproximado de 3.

[†] Trabajo de Grado

[‡] Facultad de Ingenierías Fisicoquímicas. Escuela de Ingeniería Química. Director Víctor Gabriel Baldovino Medrano, Ingeniero Químico, PhD. Codirectores: Iván Darío Mora Vergara, Ingeniero Químico, MSc.; César Augusto Luna Cáceres, Químico, MSc.

Abstract

Title: An analysis of the catalytic performance of Ni supported in hydrotreating[†].

Author: Rodrigo Valderrama Zapata[‡].

Keywords: metallic nickel, hydrotreating, hydrodesulfurization, hierarchical zeolite, strong electrostatic adsorption.

Description:

Fuel consumption around the world continues to increase. The combustion of these can generate gaseous compounds such as sulfur oxides (SO_x) that are highly polluting for the environment and harmful to health. To try to mitigate this negative impact, it opts to carry out to perform processes such as hydrotreatment (HDT), in order to remove molecules that can contribute to these repercussions. The purpose of this work was to explore the catalytic behavior of Ni supported in several aluminosilicates, especially on a hierarchical Y-type zeolite, in hydrotreatment reactions. For this, 4 supports were used: silica of low surface area, commercial alumina, commercial Y-type zeolite, and the last one, but its structure was modified in order to generate the existence of micropores and mesopores simultaneously. These supports were impregnated with Ni by the strong electrostatic adsorption method (SEA). The physicochemical properties of both the supports as the catalysts were evaluated and, finally, they were tested on hydrodesulfurization (HDS) reactions of dibenzothiophene (DBT) with and without the presence of the indole such as nitrogenous compound. The results showed that the use of the micro-mesoporous zeolite like as support obtained the highest activity results, while that the conversion with the silica and the alumina decreased about to cero after the second hour of reaction. Likewise, it observed that the presence of a nitrogenous compound promotes the HDS of the DBT, increasing the conversion by a factor of 3, approximately.

[†] Bachelor Thesis.

[‡] Facultad de Ingenierías Fisicoquímicas. Escuela de Ingeniería Química. Advisor Víctor Gabriel Baldovino Medrano, Chemical Engineer, PhD. Co-advisors: Iván Darío Mora Vergara, Chemical Engineer, MSc.; César Augusto Luna Cáceres, Chemist, MSc.

Introduction

The production of oil in Colombia is expected to reach 860,000 barrels per day (BPD) in 2020 (López S., 2019). Likewise, fuel consumption in the country continues to increase with an average demand of 177,046 BPD of diesel and 139,256 BPD of gasoline projected by 2020 (MINMINAS & UPME, 2016). However, the Colombian crude is considered a heavy oil (Ecopetrol S.A., 2014; Yáñez, Ramírez, Uribe, Castillo, & Faaij, 2018), i.e., it contains high concentrations of elements such as sulfur (S), oxygen (O), and nitrogen (N) and metals such as iron (Fe), nickel (Ni), and vanadium (V) (Alboudwarej, et al., 2006; Ramérez-Corredores & Borole, 2007). Since the combustion of this type of fuels produces pollutant gas emissions, especially sulfur oxides (SO_x), nitrogen oxides (NO_x), carbon monoxide (CO) and volatile organic compounds (VOCs) (EPA, 2017; Fan, Perry, Klemeš, & Lee, 2018), it is necessary to search for technologies and processes that allow compliance with Colombian regulations, e.g. Ley 1205 of 2008 and Resolution 182087 of 2007. These regulations seek to improve the quality of diesel and to establish that for all transport systems that use diesel, the sulfur content must not exceed 50 ppm (Ley 1205, 2008; Resolución 182087, 2007).

Hydrotreating (HDT) is a process in which about 90% of the above-mentioned pollutants are removed from the liquid fractions of petroleum. In turn, HDT can be subdivided into hydrodearomatization (HDA), hydrodemetallization (HDM), hydrodesulfurization (HDS), and hydrodenitrogenation (HDN), depending on the target pollutant (Barbosa, Vega, & Amador, 2014; Kanda, Kawanishi, Tsujino, Al-otaibi, & Uemichi, 2018).

HDS is a catalytic process that aims to remove sulfur heteroatoms present in refined petroleum products, generating hydrogen sulfide (H_2S) and organic compounds such as biphenyl (BP). In HDS, the most difficult compounds to remove are the dibenzothiophenes (DBTs) (Shafi &

Hutchings, 2000) and the alkyl-substituted DBTs, mainly in positions 4 and 6 (Jiménez, 2007), which are the most recalcitrant to HDT (Beltrán & Sarmiento, 2008). Dibenzothiophenes undergo HDS via two reaction pathways (see Figure 1); one is the mediated by the hydrogenation of the aromatic ring (HYD) and the other is the direct desulfurization (DDS) (Broderick & Gates, 1981; Egorova & Prins, 2004a). DBT is converted predominantly via the DDS pathway, whereas 4,6-substituted DBT reacts mainly via the HYD pathway (Kabe, Ishihara, & Tajima, 1992; Ma, Sakanishi, & Mochida, 1996; Bataille, et al., 2000; Macaud, Milenkovic, Schulz, Lemaire, & Vrinat, 2000; Egorova & Prins, 2004b). The difficulty in converting alkyl-substituted DBTs is due to the steric hindrance of alkyl groups, which are close to the sulfur atom and prevent the interaction of the sulfur atom with the active site (Egorova & Prins, 2004a).If the HYD pathway is favored in the HDS of DBT, then the catalyst can also transform the alkyl-substituted DBTs by this pathway (Jiménez, 2007).

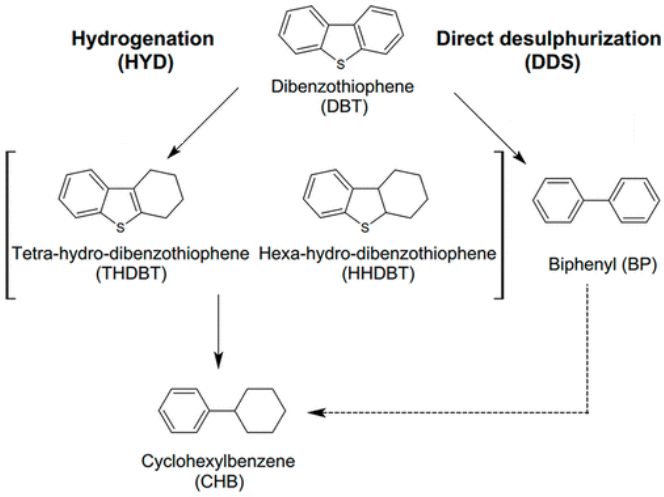

Figure 1. Reaction Network for the hydrodesulfurization of dibenzothiophene. Modified from (Morales-Valencia, Castillo-Ariza, Giraldo, & Baldovino-Medrano, 2018).

In HDN, the nitrogen heteroatom from the organic compounds present in petroleum products is eliminated as ammonia. Nitrogen organic compounds lead to the emission of nitrogen oxides (NO_x) in combustion engines (LEXICOOL; Álvarez, Hoyos, & Zambrano, 2012). HDN reactions

require much higher hydrogen pressure as compared to HDS because of the larger aromaticity of the rings containing nitrogen as compared to those containing sulfur (Jiménez, 2007). Thus, HDN is the most difficult reaction in the HDT process, and little is known about which N-compounds are the most problematic or about the kinetics of their conversion during HDN processes (Zeuthen, Knudsen, & Whitehurst, 2001). However, it is often considered that N-compounds are strong inhibitors of HDT catalysts (Zeuthen, Knudsen, & Whitehurst, 2001; Koltai, et al., 2002; Tao, et al., 2017; García-Gutiérrez, Laredo, Fuentes, García-Gutiérrez, & Jiménez-Cruz, 2014; Rana, Al-Barood, Brouresli, Al-Hendi, & Mustafa, 2018). Nevertheless, in recent studies in our research group (Centro de Investigación en Catálisis, CICAT, per its acronym in Spanish), have found that nitrogen compounds can promote HDS via the DDS pathway (Morales-Valencia E. M., 2019). Therefore, this promotion effect needs to be studied more thoroughly (Jiménez, 2007).

Currently, many catalysts have been proposed for HDT (Breysse, Afanasiev, Geantet, & Vrinat, 2003; Breysse, Geantet, Afanasiev, Blanchard, & Vrinat, 2008; Nikulshin, et al., 2016; Huirache-Acuña, Gabriel Alonso-Nuñez, Rivera-Muñoz, & Pawelec, 2016) (view Table 1). However, alumina (Al_2O_3) (Beltrán & Sarmiento, 2008; Arias & Lozano, 2008; Baldovino-Medrano, Giraldo, & Centeno, 2009) supported Co or Ni promoted molybdenum sulfides -Co(Ni)-MoS_2/Al_2O_3)- dominate the industry (Kanda, Kawanishi, Tsujino, Al-otaibi, & Uemichi, 2018; Beltrán & Sarmiento, 2008; Egorova & Prins, 2004a; Okamoto, 2008; Tang, et al., 2013) due to their high performance and stability. The Co(Ni)-MoS_2 active phase has also been supported on amorphous (ASAs) (Pérez, Gaigneaux, Giraldo, & Centeno, 2011) or crystalline, i.e. zeolites, aluminosilicates (Tang, et al., 2013), leading to catalysts with different physicochemical properties, among which acidity is key. Table 1 summarizes some of the most studied catalysts in HDT.

Table 1.
Summary of catalysts used often in HDT, especially HDS.

Active phase	Support	Reference	Active phase	Support	Reference
Sulfided CoO-MoO_3	γ-Al_2O_3	(Broderick & Gates, 1981)	Metallic Pt	ASA	(Reinhoudt, et al., 1999)
Sulfided CoO-MoO_3 Sulfided NiO-MoO_3	Al_2O_3	(Furimsky & Massith, 1999)	Sulfided and metallic Pt, Pd, and Ru – Mo	γ-Al_2O_3	(Meriño, Centeno, & Giraldo, 2000)
Sulfided CoO-MoO_3 Sulfided NiO-MoO_3 Sulfided MoO_3	γ-Al_2O_3	(Egorova & Prins, 2004a)	Sulfided CoO-MoO_3	---	(Okamoto, 2008)
Reduced PtPd	γ-Al_2O_3	(Baldovino-Medrano, Eloy, Gaigneaux, Giraldo, & Centeno, 2009)	Sulfided PtMo	γ-Al_2O_3-B_2O_3	(Baldovino-Medrano, Giraldo, & Centeno, 2009)
Sulfided CoO-MoO_3 Sulfided NiO-MoO_3	Sodalite[a]	(Leonardo, Álvarez, Ocanto, & Linares, 2011)	Sulfided CoO-MoO_3	ASA	(Pérez, Gaigneaux, Giraldo, & Centeno, 2011)
Metallic Pd	HY-M[b]	(Fu, et al., 2011)	Sulfided NiO-MoO_3	Al_2O_3 TiO_2-Al_2O_3	(Vázquez, López, Berhault, & Guevara, 2019)
Sulfided CoO-MoO_3	NB-MOR[c]	(Tang, et al., 2013)	Sulfided CoO-MoO_3	ZSM-5[d] Faujasite	(Yocupicio, Díaz de León, Zepeda, & Fuentes, 2017)
Sulfided NiO-MoO_3	Al_2O_3-SiO_2	(Wang, et al., 2017)	Rh, Pd and Ru Phosphides NiMoS	SiO_2	(Kanda, Kawanishi, Tsujino, Al-otaibi, & Uemichi, 2018)
Metallic Ni	Al_2O_3	(Zhao, et al., 2019)			

[a] Light Blue Ultramarine (silicate), [b] Y – Mesoporous Zeolite, [c] Mordenite Nanofiber Bundles, [d] Zeolite Socony Mobil # 5.

Zeolites are microporous (average pore diameter <2 nm) acidic materials (Brönsted acids, mainly), widely used as catalysts and supports for heterogeneous catalysts (Garnica, 2016; Grau, 2016). Though their porosity and acidity are key in many of its applications, their application in hydrotreating (Yocupicio, Díaz de León, Zepeda, & Fuentes, 2017) is limited by the poor diffusivity of DBTs to their active sites (Perez-Ramirez, Christensen, Egeblad, Christensen, & Groen, 2008); in average, DBTs have molecular diameters around 1.16 nm (Moosavi, Dastgheib, & Karimzadeh, 2012).

An alternative to improve the diffusivity of DBTs into the pores of the zeolites is to generate mesopores in the zeolite. When these mesopores make regular channels that connect directly with the micropores of the zeolites (see Figure 2), the material is classified as a hierarchical zeolites (Feliczak-Guzik, 2018; Van Aelst, et al., 2015). These zeolites have advantages associated with each level of porosity, from selectivity to mass transport (Chen, et al., 2012). They are thus interesting for the hydrotreatment of heavy oils, that contain mostly bulky molecules, because of the possibility of reducing diffusional problems in the reactor (Grau, 2016). Also, the use of this type of zeolites as support for Pd catalysts increased ca. 36% the conversion of alkyl-DBTs when compared with the Pd catalyst supported on the microporous zeolite (Fu, et al., 2011).

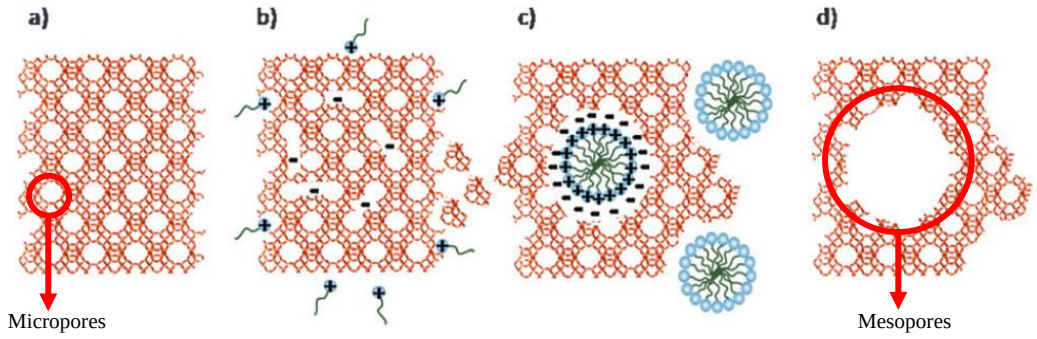

Figure 2. Schematic of the Speculated Zeolite Mesopore Formation Process: (a) Original Zeolite Y, (b) Si–O–Si Bond Opening/Reconstruction in Basic Media, (c) Crystal Rearrangement to Accommodate the Surfactant Micelles, and (d) Removal of the Template to Expose the Mesoporosity Introduced. Modified from (García-Martínez, Johnson, Valla, Li, & Ying, 2012).

In this work, we study the performance of nickel supported on different oxide supports, including: silica, alumina, microporous H-Y zeolite, and a mesostructured H-Y zeolite. We chose to work nickel because of its hydrogenating nature (Adkins & Cramer, 1930) and its lower cost when compared with platinum or palladium (Glacier RIG, 2020; GREENWOOD & EARNSHAW, 1997). As we mentioned earlier, Ni is a promoter of MoS_2 in hydrotreating catalysts often disregarded as a potential monometallic active phase (Kanda, Kawanishi, Tsujino, Al-otaibi, & Uemichi, 2018; Song, 2003). There are two reasons for this: (i) Ni has a strong tendency to form

HDT inactive $NiAl_2O_4$ aluminates with the alumina support; and, (ii) it is considered that metallic nickel is easily transformed into a poorly active nickel sulfide under the HDT reaction environment (Chianelli, 2006). Therefore, the exploration of the use of monometallic nickel as catalyst in HDT process is a curiosity only reported,as far as we know, by Zhao et al. in 2019 (Zhao, et al., 2019). The cited study established that alumina supported reduced nickel species are active in the hydrodesulfurization of thiophene at 370°C. Thus, there is a lot to learn about the behavior of monometallic supported Ni catalysts in HDS and HDN. Herein, we analyze the effect of the support on the catalytic performance of monometallic Ni used in HDT.

1. Objectives

1.1. General Objective

To analyze the catalytic behavior of aluminosilicate supported metallic Ni catalysts in HDS and HDN reactions.

1.2. Specific Objectives

To determine the physicochemical properties of the catalysts that are relevant for their catalytic behavior.

To evaluate the effect of different supports on the catalytic behavior of monometallic nickel in HDS and HDN reactions.

To correlate the physicochemical properties of the catalysts with their reactivity.

2. Experimental

2.1. Pretreatment of the catalytic supports

The following materials were used to obtain the catalytic supports: sodium loaded silica (Na-SiO_2, Commercial Grade), extruded alumina (Al_2O_3, Sasol), and, a Na-Y zeolite powder with nominal molar ratio Si/Al ~ 2.6 (Aldrich).

2.1.1. Pretreatment of the SiO_2 and Al_2O_3 supports. The sodium loaded SiO2 was washed for 24 h, by the reflux method (Project, Provost, Library, Program, & Merlot, 2019), with a 1M solution of hydrochloric acid (HCl, Merck-37% fuming), using a ratio of 100 g of SiO2 • L-1 of acid solution, in order to remove the sodium. For this, a flat-bottomed flask containing the mixture was placed in a sand bath heated at 68°C. The mouth of the flask was connected to a Friedrichs condenser. The SiO2/HCl mixture was stirred at 100 rpm with a magnetic stirrer. After washing, the recovered silica particles were filtered using filter paper and thoroughly washed with type I water until a neutral pH was reached. Finally, the sodium free silica was dried at 80°C for 18h in

a static oven (Precision Premium Mechanical Convection - PR305045M, Thermo Scientific). On the other hand, the extrudates of alumina were crushed with mortar and pestle and then sieved to a particle size between 25-75μm. This particle size was the same of the other catalytic supports.

2.1.2. Mesoporous generation in Na-Y zeolite and ionic exchange. A meso-microporous Na-Y zeolite was synthesized adapting the surfactant-templating method of García-Martínez (Sachse, et al., 2017). For this purpose, a 40% suspension of the zeolite in water was made. Then, a 0.1M solution of citric acid ($C_6H_8O_7$, Merck, 99%) was added dropwise to the suspension. Under such conditions, a zeolite/solution ratio of 167 g NaY • L^{-1} acid solution was obtained. The suspension was maintained under constant stirring at 200 rpm for 1 h. The thus treated zeolite was recovered and washed with type I water, until a neutral pH was reached. The recovered powder was further dried for 2 h at 60°C. The dried powder was then dispersed in an aqueous solution of 0.22 M of hexadecyltrimethylammonium bromide, CTAB, and 0.025 M of NaOH as to obtain a zeolite/total solution ratio of 85 g of NaY • L^{-1} of solution. The suspension was stirred at 350 rpm for 20 min. Afterwards, the produced slurry was transferred to a *Teflon-Lined Stainless-Steel Autoclave* reactor and put in an oven at 150 ° C for 15 h. After removing the reactor from the oven and allowing its cooling for 15 min, the material was mixed with a methanol (brand, purity)-water (type-I) solution to be further centrifuged in a *LC-04R* (Zenithlab) apparatus. The recovered solid was dried at 40°C for 1 h. Finally, the recovered zeolite was calcined at 550°C with a ramp of 1.5°C•min^{-1} using a *CWF 1200* (Carbolite) furnace. This zeolite was called NaY-M.

Both the NaY and the NaY-M zeolites were transformed into their acid forms by ion exchange (Liu, et al., 2020) with an ammonium nitrate solution (NH_4NO_3, PanReac AppliChem - 99%). For this purpose, a zeolite/solution ratio of 10 g • L^{-1} suspension was made and stirred at 300 rpm at room temperature for 8 h. Finally, the exchanged zeolites were filtered and allowed to dry at 60°C

overnight. The ion exchange was repeated thrice. After the third exchange, the zeolites were calcined at 550°C for 6 h with a ramp of 2°C•min^{-1}. The thus pretreated zeolites were called HY and HY-M.

2.2. Characterization of the Supports

2.2.1. Determination of the Point of Zero Charge (PZC). PZC is defined as the condition at which the average surface charge density of an oxide equals zero (Park & Regalbuto, 1995; Kosmulski M. , 2009). This property was determined by the Immersion Technique (Fiol & Villaescusa, 2009); also known as the Drift Method (Pashai, Moghaddam, & Ghorbani, 2016). For the method, a 0.01M solution of sodium chloride (NaCl, Merck - 99.5%) was prepared and divided equally into six beakers. Then, using 0.01M NaOH or HCl solutions, the pH was adjusted to obtain values between 2 and 12. pH was read using a *HI 5522* (Hanna Instruments) pH meter, and the initial value recorded for the experiments was called $\boldsymbol{pH_{initial}}$. Next, adequate amounts of each solid were added to the solution to sequentially make 3 mg sample • mL^{-1} of solution suspensions every time. These suspensions were stirred at 200 rpm at room temperature for 24 h. The pH recorded after these treatments was called $\boldsymbol{pH_{final}}$. With these data, a curve of $\boldsymbol{\Delta pH\ vs\ pH_{initial}}$ was plotted, where $\boldsymbol{\Delta pH = pH_{final} - pH_{initial}}$, and finally, the $\boldsymbol{PZC = pH_{PZC}}$ was determined as the pH at which the curve intersects the abscissa axis, i.e., when $\boldsymbol{\Delta pH = 0}$.

2.2.2. Determination of the surface area and porosity of the materials. These properties were calculated with data from argon adsorption and desorption isotherms measured at -186.15°C. Samples were weighed in 9 mm diameter cells made of borosilicate glass. Samples of ca. 0.1g were used for the zeolites, whereas ca. 0.15g were used for both the Al_2O_3 and the SiO_2 supports. Before each analysis, powders were degassed for 2 h at 120°C and then for 6 h at 300°C in order to remove any type of impurities adsorbed on their surface. This procedure was performed with a

Vac Prep 061 (Micrometrics) device. Isotherms were measured in a *3FLEX*^{TM} (Micrometrics) apparatus in a relative pressure (P/P_0) range between 1.0×10^{-4} and 0.993. Data analysis was performed with the *3FLEX V.4.03* (Micrometrics) software. The specific surface areas of the samples were calculated by the BET method (Brunauer, Emmett, & Teller, 1938), whose application interval was adjusted according to the consistency criteria of the Rouquerol transform (Rouquerol, Rouquerol, Llewellyn, Maurin, & Sing, 2013). Pore size distributions were estimated by the Non-Local Density Functional Theory (NLDFT) (Jaroniec, Kruk, Olivier, & Koch, 2000) for the micropores region and by the BJH method for the mesopores region (Barrett, Joyner, & Halenda, 1951). Calculation routines for the BET, NLDFT, and BJH methods are included in the *3FLEX V.4.03* software.

2.2.3. Determination of the distribution of surface hydroxyls. Proton Affinity Distributions (PADs) were calculated for assessing the relative concentration of the surface hydroxyls groups of the supports (Contescu, Jagiello, & Schwarz, 1995; Restrepo-Garcia, Ramírez, & Baldovino-Medrano, 2018). Measurements were made by potentiometric titration with a *pH Module 867* (Metrohm). For the tests, ca. 0.1 g of the samples were added to 30 mL of a 0.1 N aqueous solution of sodium nitrate ($NaNO_3$, Merck, 99.5%). The obtained suspension was homogenized by magnetic stirring for 60 min. For titration in the pH basic range, a 0.05 N aqueous solution of NaOH was used as a titrating agent. Titration was made by automatically dosing 0.05 mL of the NaOH solution each 20-90 s until a pH of 10.9 was reached. Likewise, titration was performed in the acidic range for a fresh sample with a 0.037 N nitric acid (HNO_3, Merck - 65% v/v) aqueous solution until a pH of 3.0. pH. The changes in pH were measured in terms of the volume (basic or acidic) of the solution added. The acquired data were used to construct a proton consumption function $\boldsymbol{f(Log\ K)}$ as a function of pH by a proton balance (Contescu, Jagiello, & Schwarz, 1993;

Contescu, Popa, Miller, Ko, & Schwarz, 1995; Pérez-Martínez, Acevedo-Quiroga, Giraldo-Duarte, & Centeno-Hurtado, 2011; Morales, Mora, Giraldo, & Centeno, 2011).

2.3. Impregnation of Ni

Catalysts were synthesized by adapting the Strong Electrostatic Adsorption (SEA) method (Cho H. R., 2013; Cho & Regalbuto, 2015). This method is based on the fact that when an oxide in suspended in an aqueous solution, its surface acquires either a negative or positive net charge as a function of the pH in relation to the PZC of the oxide. Namely, when the pH of the impregnating solution is above the PZC of the oxide, its surface hydroxyl groups protonate and become positively charged hence favoring the adsorption of anionic metal complexes from the impregnating solution. Conversely, if the pH is above the PZC, the hydroxyl groups from the oxide de-protonate and the surface of the oxide becomes negatively charged hence promoting the selective adsorption of cations from the impregnating solution (Regalbuto, 2006) (see Figure 3a). For applying the method, one also needs to consider that the maximum density for an adsorbed ion complex with a *2-* charge corresponds to a close-packed monolayer of complexes that retain one hydration sheath, which corresponds to the surface hydroxyls density, as depicted in Figure 3b for the particular case of platinum impregnation.

Following the rationale described above, the impregnation of Ni over the selected supports was carried out as follows. First, we calculated, see Equation C.1 in Appendix C for details, the adequate loading of nickel aiming to achieve a statistical monolayer of the metal over the silica support; i.e. the support with the lowest surface area, see the Results section. Accordingly, we calculated the corresponding weight of the nickel precursor: nickel nitrate hexahydrate ($Ni(NO_3)_2 \times 6H_2O$, Merck - 99%) and dissolve it in type I water. The volume of this solution was equal to six times the estimated pore volume of the corresponding support. Then, the necessary

stoichiometric amount of an ammoniacal solution (NH_4OH, Merck - 25-30% v/v), according to Equation C.7 – Appendix C, was added dropwise to obtain the $[Ni(NH_3)_6]^{2+}$ complex ion after setting the pH between 11.6-11.8. Then, the powdered supports were contacted with the impregnating solution and each suspension was left under stirring at 200 rpm for 1 h. Afterwards, these suspensions were filtered and washed with type I water four to five times. Following each impregnation, the solids were dried overnight at 90°C.

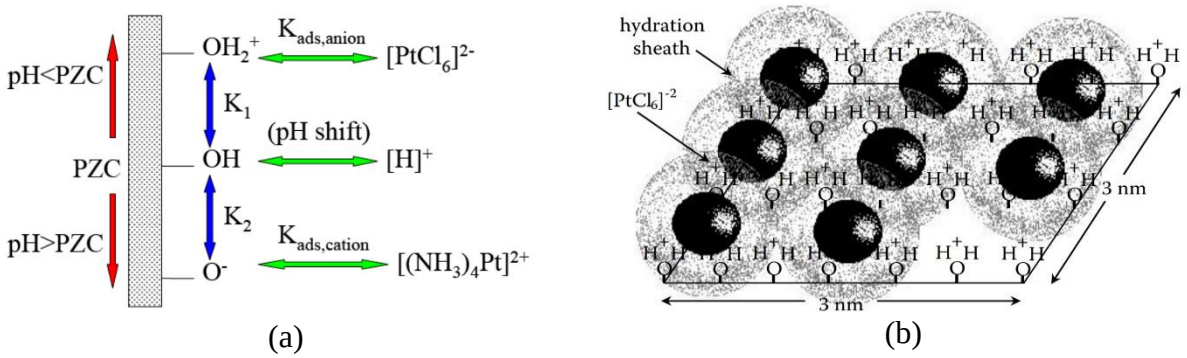

Figure 3. Electrostatic Adsorption Mechanism; (a) Surface Charging, Metal Adsorption, and Proton Transfer (Cho H. R., 2013), and, (b) Monolayer Coverage of Pt Anions with Hydration Sheath (Regalbuto, 2006).

For defining the heat treatment conditions of the impregnated solids, we performed a thermogravimetry analysis (TGA) of the fresh solids using a *Discovery 5500* (TA Instruments). To do this, about 10 mg of each sample were weighed and put into the instrument where they were heated from 25°C to 800°C by a ramp of 5°C•min^{-1}, under an air flow (99.997%) of 25mL•min^{-1}. The data were analyzed with the *Trios v4.4.0.41128* (TA Instruments) software. With this information (Appendix G), the catalysts were roasted using two sequential heating stages: the first was by heating to 300°C and holding this condition for 1 h. The second was by heating to 450°C for 4 h. In each case, a 2ºC•min^{-1} ramp was used. Finally, the catalysts synthesized by the above methods were named: Ni/Al_2O_3, Ni/SiO_2, Ni/HY and, Ni/HY-M, according to the used support.

Aside from the above catalysts, another catalyst, used as a reference, with the same nickel loading and supported over HY-M was prepared using the incipient wetness impregnation method proposed by (United States Patent No. 4.801.573, 1987). For this purpose, the same Ni precursor used before was dissolved in the given volume of water and put into contact with the established amount of support to be impregnated. The mixture was stirred for 1 h and then left to rest for 18 h at room temperature. Subsequently, the excess water was dried, and the recovered solid was thermally treated in the same fashion as it was made for the other catalysts. This catalyst was called Ni/HY-M*.

2.4. Characterization of the catalysts

The surface area, volume and pore size distribution were determined for all catalysts (except Ni/HY-M*) from Ar physisorption tests, as mentioned in section 3.2.2. Likewise, the distribution of their surface hydroxyls was analyzed using the methods explained in section 3.2.3. Finally, the loading of Ni were measured by flame atomic absorption spectrometry, where approximately 0.2g of each catalyst were subjected to an acid digestion process (Westerman, RuffioM, Wainwright, & Foster, 1980) with 1.5 mL of sulfuric acid (H_2SO_4, Merck - 65% v/v) added dropwise. Subsequently, the samples were treated with 2 mL of hydrofluoric acid (HF, Merck - 80%) at 80°C for about 15 min. At this point, all sulfur trioxide fumes came out (Westerman, RuffioM, Wainwright, & Foster, 1980). Finally, 100 mL of type I water were added to the samples to complete the dissolution process.

2.5. Catalytic tests

Catalytic tests were carried out in a Catatest (Morales-Valencia E. M., 2019; Baldovino-Medrano, Eloy, Gaigneaux, Giraldo, & Centeno, 2009), vide Figure K.1. in Appendix K, provided with high-pressure fixed-bed continuous flow reactor operated in integral mode. The reactor was

packed with the catalyst. Prior to the latter, the catalytic powders were pelletized, ground and sieved to obtain particles with diameters ranging from 300 to 600 μm. For the catalytic tests, ca. 0.50 g (see Table K.1. - Appendix K), were dried in situ under N_2 flow (100 mL•min^{-1}) at 120°C for 1 h. Afterwards, the catalyst was activated during 4 h using a H_2 volumetric flow rate of 100 mL•min^{-1} at atmospheric pressure and 400°C. After activation, reactants were fed into the reactor at a volumetric flow rate of 30 mL•h^{-1}. Then, the reactor pressure was increased with H_2 to 5 MPa and the liquid feed was pumped up to the reactor. A hydrogen/(liquid feed) rate ratio of 500 NL • L^{-1} was fixed for the experiments. Reaction temperatures were programmed to start at 300°C, to stabilize the catalyst. Reaction tests were conducted until reaching steady state; i.e. between 5 and 8h. The reaction feedstock accounted for the following compounds employed either individually or in blends: dibenzothiophene (DBT, Sigma-Aldrich, 98%), as a model sulfur compound, and indole (IND, Sigma-Aldrich, ≥99%), as a model for heterocyclic nitrogen compounds. Hexadecane (Sigma-Aldrich, 99%) was used as an internal standard for chromatography, and cyclohexane (CH, Sigma-Aldrich, 99.8%) was used as solvent. For all tests, 2.2 wt.% DBT were put into the liquid feed. On the other hand, a S/N molar ratio equal to 5 was fixed for those tests with DBT and indole.

The identification and quantification of the liquid reaction products were made by the gas chromatography (GC) and GC mass spectroscopy (GC-MS) techniques. Gas chromatography analyses were performed with a *HP 6890* chromatograph equipped with an FID detector and an automatic injector. An *HP-1* column (Agilent J&W, 100 m × 0.25 mm × 0.5 μm) was used for both GC and GC-MS. The analysis conditions were as follows: the GC oven temperature was programmed from 90 to 180°C (15 min) at 30°C•min^{-1}, then to 260°C (10 min) using a temperature ramp of 30°C•min^{-1}. We used a H_2 flow of 50 mL•min^{-1}, an air flow of 500 mL•min^{-1}, and helium (Linde Colombia S.A, 99.99%) as carrier gas, with 19 cm•s^{-1} linear velocity (1.1 mL•min^{-1}, at

constant flow). The compounds in each sample were identified by comparing their retention times with those of standards, and the quantification was carried out using calibration curves.

In general, the catalytic results were expressed in terms of reactants conversion (%X_i), products selectivity (%S_j), and yield (%Y_j) percentages, as follows:

$$\%X_i = \frac{n_{i_{initial}} - n_{i_{final}}}{n_{i_{initial}}} * 100 \quad \text{Eq. 1}$$

Where, $n_{i_{initial}}$ and $n_{i_{final}}$ are the initial and final moles of the reagent (i), respectively.

$$\%Y_j = \frac{n_j}{n_{i_{initial}}} * 100 \quad \text{Eq. 2}$$

$$\%S_j = \frac{n_j}{\sum n_j} * 100 \quad \text{Eq. 3}$$

Where, n_j are the moles of the product j.

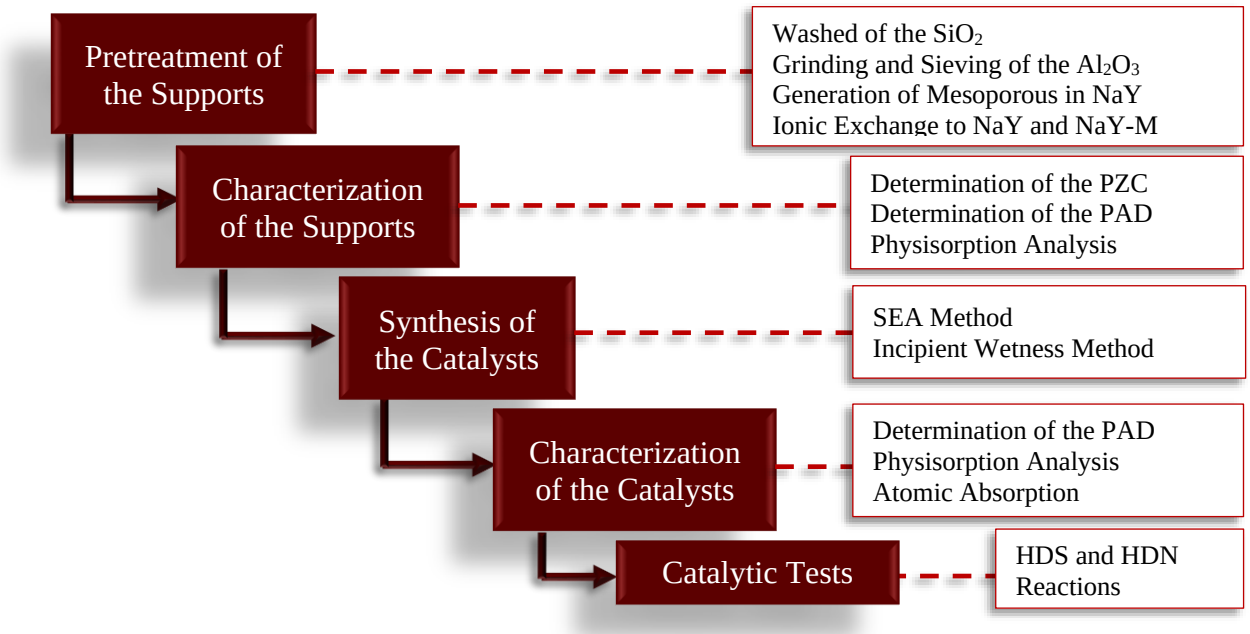

Figure 4. Summary of the methodological approach of this work.

3. Results

3.1. Physicochemical properties of the supports

The physicochemical properties of the pretreated supports are discussed below.

3.1.1. Point of zero charge of the supports. Table 2 presents the values of pH where the PZC for each one of the pretreated supports. For SiO_2, instead of a single pH value, we report a pH range between 3.0 – 4.0 because, the conditions of our experiments, the $\Delta \boldsymbol{pH\ vs\ pH_{initial}}$ curves were superimposed below pH ~3.0 hence making unfeasible to find a precise $\boldsymbol{pH_{PZC}}$ value. However, the measured $\boldsymbol{pH_{PZC}}$ range is consistent with the reports from literature (Kosmulski M. , 2009; Kosmulki, 2001; Abendroth, 1970; Yates & Healy, 1976; Noh & Schwarz, 1989). For Al_2O_3, the $\boldsymbol{pH_{PZC}}$ value was around 7.0 indicating that it has a neutral surface (Das, Sahu, Borthakur, & Mahiuddin, 2004) and its value is according with the PZC of others aluminas with similar physical properties (Contescu, Jagiello, & Schwarz, 1993; Contescu, Contescu, & Schwarz, 1994; Trueba & Trasatti, 2005; Greenwood, 2003). However, the herein found PZC is lower than the average of those published in literature (Kosmulski M. , 2001) which indicates that our alumina has fewer surface hydroxyls groups (Das, Sahu, Borthakur, & Mahiuddin, 2004). On the other hand, the PZC value for the microporous HY zeolite was lower than the one of the micro-mesoporous HY-M zeolite. The acidic values of the PZC for SiO_2, HY zeolite, and the HY-M zeolite are due to the presence of surface acid sites that are either of the Brönsted type or related. Brönsted acid sites consists of a polarized hydrogen atom which is bonded to an oxygen atom connecting tetrahedrally coordinated cations (Deka, 1998; Busca, 2017).

Table 2.
Physical properties of the SiO_2, Al_2O_3, HY zeolite, and HY-M zeolite.

Sample	SA_{BET} [$m^2 \cdot g^{-1}$]	SA_{Micro} [$m^2 \cdot g^{-1}$]	SA_{Meso} [$m^2 \cdot g^{-1}$]	PV_{NLDFT} [$m^3 \cdot g^{-1}$]	PS_{NLDFT} [nm]	PS_{BJH} [nm]	PZC	OH density [$OH \cdot nm^{-2}$]	OH concentration [$mmol \cdot g^{-1}$]
SiO_2	14	4	10	0.08	1.3	11.2	3.0-4.0	>7.5	0.17
Al_2O_3	128	--	128	0.44	1.3	11.8	7.1	<8.4	1.78
H-Y	870	788	83	0.36	0.8	--	3.3	>0.9	1.34
HY-M	789	557	231	0.42	0.8	3.2	4.9	<1.3	1.66

Note: With this information, it was possible to establish the electrostatic conditions and the nickel precursor salt to do the impregnation by the SEA method.

3.1.2. Specific surface area and porosity. Figure 5 shows the Ar adsorption-desorption isotherms recorded for each one of the pretreated supports. For both SiO_2 and Al_2O_3 (Figures 5a and 5b, respectively), type IV isotherms were found, which are typical of mesopore materials (López, 2004). According to the IUPAC (Thommes, et al., 2015), the hysteresis loop that is visualized in Figure 5a is of type H_2(b), and is attributed to pores formed by the agglomeration of spherical particles, or also by the presence of capillaries with a very heterogeneous distribution of sizes and geometries (Martín-Martínez, 1990). On the other hand, for alumina, the hysteresis cycle is of the H_1 type, which is characteristic of closed and open cylindrical pores (López, 2004).

For the HY zeolite (Figure 5c), a type I isotherm was found, which is typical of microporous solids (López, 2004). In contrast, the micro-mesoporous HY-M zeolite, Figure 5d, showed an isotherm which is a combination of type I and IV isotherms (Thommes, et al., 2015), thus demonstrating the simultaneous presence of micropores and mesopores. Furthermore, the formed hysteresis loop appeared between P/P_0 = 0.3 - 0.6, which represents the formation of open mesopores connected with the inner micropores of the zeolite (Sachse, et al., 2017). Table 2 shows the values for the BET specific surface area (SA_{BET}), micropore surface areas (SA_{Micro}), mesopore surface areas (SA_{Meso}), the calculated volumes and average pore sizes (PS_{NLDFT}, PS_{NLDFT}, and, PS_{BHJ}). The corresponding accumulative pore volume curves as well as the pore size distribution curves for the supports can be viewed in Appendix D.

The data shows that the specific area for SiO_2 was the lowest among the supports, followed by Al_2O_3, HY-M, and HY. We notice that the mesoporous surface of the HY-M zeolite formed at the expense of the internal micropore specific area without destroying the zeolitic framework as evidenced by the fact that the average pore size of the micropores for both HY and HY-M is the same. Meanwhile, the formed mesopores in HY-M were almost one order of magnitude larger than

the micropores. The data presented in Table 2 was used to calculate the volumes of the impregnating solutions for synthesizing the supported nickel catalysts.

3.1.1. Distribution of surface hydroxyls. Figure 6 shows the PAD curves obtained for each one of the catalytic supports. For SiO_2, three regions were identified in the PAD curves (see Figure 6a); one at pH < 4 for protonated $SiOH_2^+$, the second at pH = 4 – 8 for SiOH; i.e. reactive silanol groups (Dias & Ribeiro do Carmo, 2006), and, the third one at pH > 10 for dehydroxylated SiO^- species.The silanol groups are fact those that convert either into $SiOH_2^+$ or SiO^- (Duval, Mielczarski, Pokrovsky, Mielczarski, & Ehrhardt, 2002). In the synthesis of the catalysts by the SEA method, the number of available surface sites for adsorbing the metallic precursor equals the number of reactive hydroxyls.

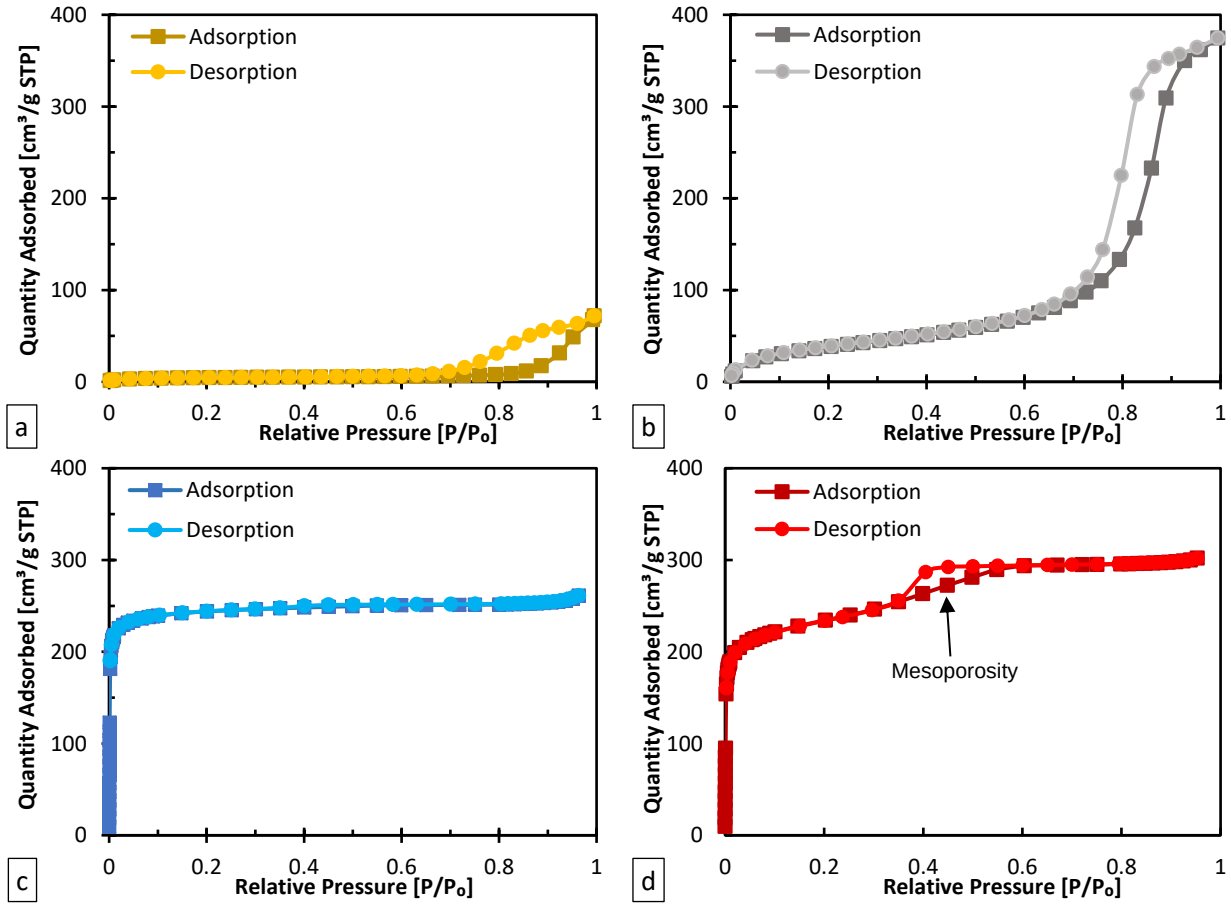

Figure 5. Ar Adsorption-Desorption Isotherms from (a) SiO_2, (b) Al_2O_3, (c) HY, and, (d) HY-M. measured at -186.15°C.

For Al_2O_3, Figure 6b, distinct types of surfaces hydroxyls were identified: namely, OH types: III, IIA, IA, and, IB sites are pointed out following the classification made by Knözinger (Knözinger & Ratnasamy, 1978) (see Figure E.1.1. and Table E.1.1. in Appendix E for details on the chemical structure of these hydroxyls). According to this classification, Type I OH groups are terminal sites either coordinated to a single tetrahedra (IA OH groups) or to an octahedral (IB OH groups) Al^{3+} cation. Type IB hydroxyls are the most acidic OH groups while Type IA are mildly acidic. Whereas, Type IIA OH groups are mildly basic and consist of bridging OH groups which link an octahedral and a tetrahedral Al^{3+} cation (Knözinger & Ratnasamy, 1978). Finally, Type III sites are the most basic ones. According to the area under the PAD curve for Al_2O_3, the relative

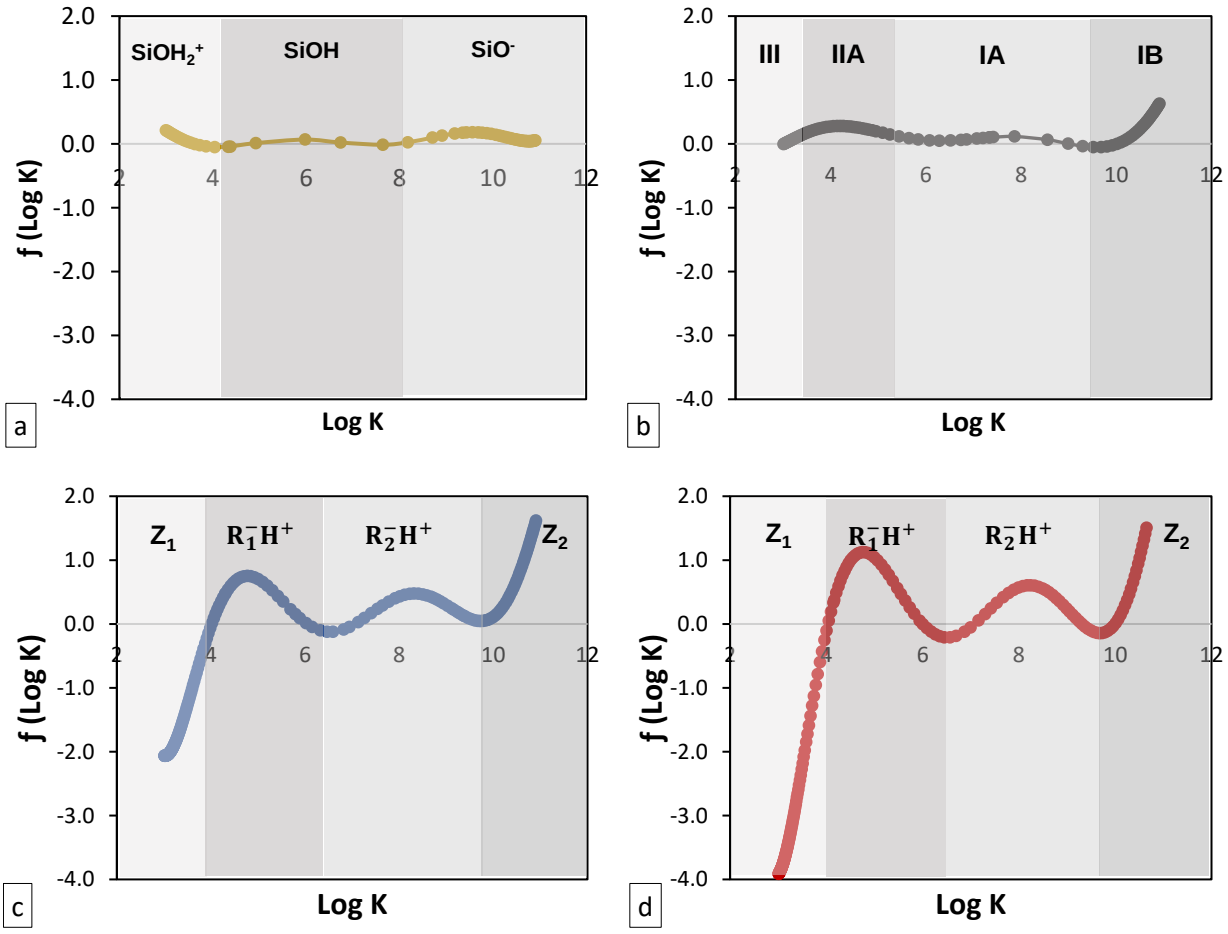

Figure 6. Proton Affinity Distribution curves for (a) SiO_2, (b) Al_2O_3, (c) HY, and, (d) HY-M.

concentration of its hydroxyls followed the order: IB > IIA > IA > III, which indicates this support primarily has strong basic OH groups followed by groups with intermediate acidity.

For the zeolites, the existence of two types of acid sites was evident (Figures 6c and 6d), which is characteristic for zeolites (Busca, 2017; Borges & Lemos de Macedo, 2016; Gackowski, et al., 2018; Zhang, et al., 2019). The first type of site, at pH = 4 – 6, and with a pKa of 5, is considered to a transition between acidic and basic, and the second, at pH = 6 – 8 and with a pKa of 8.5, is moderately acidic (Yu, et al., 2016). These sites were called $R_1^- H^+$ and $R_2^- H^+$, respectively, in the PAD plots. For the region marked as Z_2, pH > 10, the dissolution of the zeolite begins to occur (Yu, et al., 2016; Shcherban, et al., 2017). On the other hand, for the region with pH < 4, named Z_1, the negative values of the PAD function -f(log K)- can be ascribed to the denaturalization of the Brönsted acid sites of the zeolites. Therefore, the quantification of the surface hydroxyls of the zeolites was restricted to pH between 4 and 10. Comparing the samples from HY and HY-M, Figures 6c and 6d, an increase in the relative concentration of acid sites can be suggested. This is ascribed to a slight decrease Si/Al ratio of the material that follows from its desilication (Borges & Lemos de Macedo, 2016).

Values for the OH surface density of the catalytic supports are presented in Table 2. Of course, SiO_2 has a lower concentration of surface hydroxyls as compared to the other materials but, owing to its lowest surface area, the surface density of its hydroxyls is high; almost the same as the one Al_2O_3. Both SiO_2 and Al_2O_3 indeed showed the highest OH surface densities. As for the zeolites, the mesoporous structured HY-M displayed a slightly higher surface density of OH. We used this information to calculate the loading of nickel that makes a statistical monolayer over the support with the lowest surface area; i.e. SiO_2 (see Appendix F). Therefore, it can be deduced that all the

other catalysts had less than a monolayer of coverage of nickel while keeping the same metallic loading.

3.2. Physicochemical properties of the catalysts

The textural properties of the catalysts were analyzed following physisorption tests. These tests were carried out for the powders obtained after each synthesis as well as for samples taken after the pelletizing procedure made to obtain the particle size distribution required for the HDT reactions, section 3.5. Figure 7 shows the Ar adsorption and desorption isotherms measured for both the freshly synthesized powders and the particles recovered after pelletizing. We see that the catalysts kept the same porous structure before and after pelletizing. However, it is evident that the zeolites lost part of their surface area; i.e. we observe a strong decrease in the initial amount of Ar that they adsorb. On the other hand, comparing the catalysts (Figure 7) with the supports

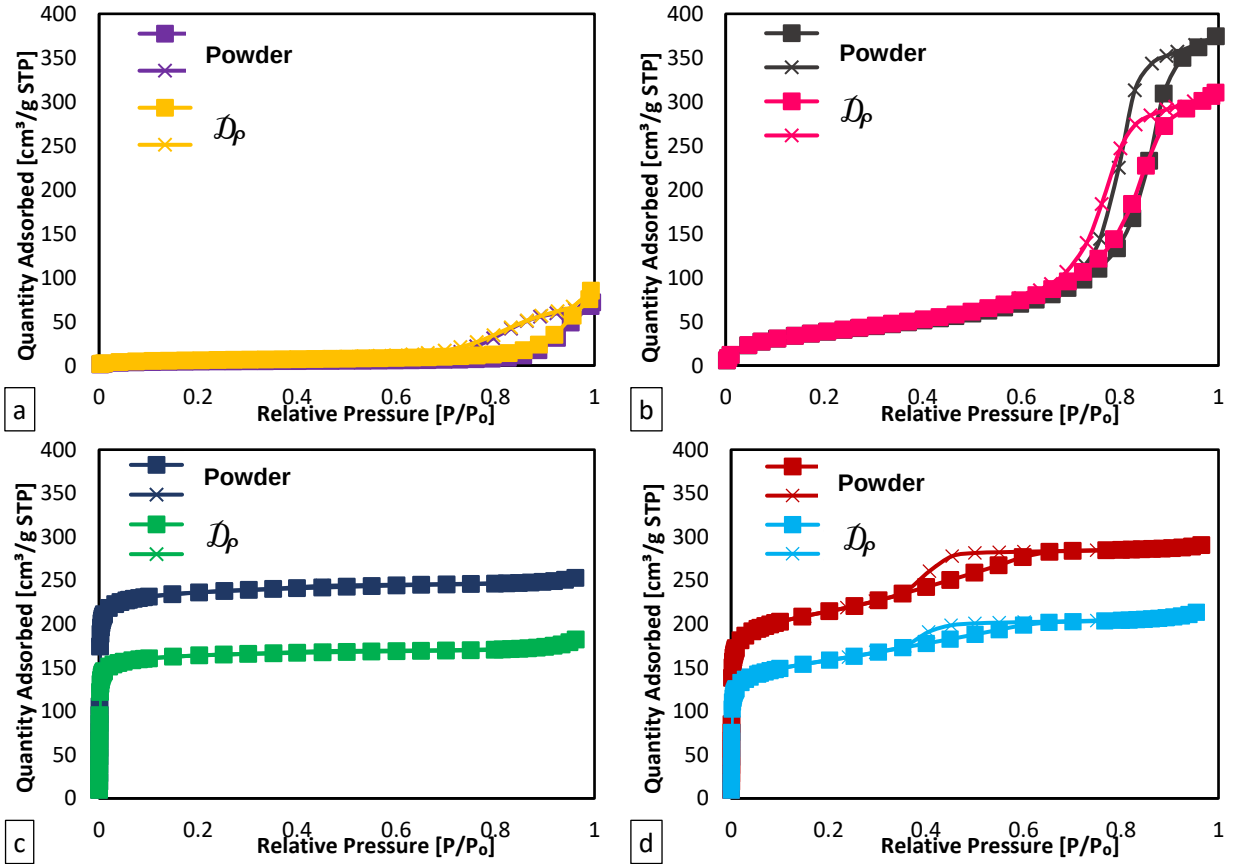

Figure 7. Ar Adsorption (■)-Desorption (×) Isotherms of the Powders and, Pelletized, Ground and Sieved ($\mathcal{D}_p$) from (a) Ni/SiO_2, (b) Ni/Al_2O_3, (c) Ni/HY, and, (d) Ni/HY-M. Measured at -186.15°C.

(Figure 5) no evident changes in both porosity and surface are were seen. This result indicates that the impregnation of Ni has a negligible on the texture of the materials. Therefore, nickel particles are expected to be highly dispersed over the supports.

Figure 8 shows the proton affinity distribution curves for the catalysts. The recorded trends showed a high consumption of surface OH groups for all catalysts prepared by the SEA method, especially for those with the lower surface areas; i.e., silica and alumina. Indeed, the PAD curves of these materials were basically flat. Instead, the PAD curves for the catalysts supported over the HY and the HY-M zeolites showed that a high number of surface hydroxyls were still free to adsorb nickel. In general, the ensemble of these results shows the high selectivity that can be achieved when impregnating a metal via the SEA method. In contrast, the Ni/HY-M* catalyst; which was prepared by the typical incipient wetness impregnation method, basically displayed the same PAD curve of the HY-M support which evidences the poor specificity of the method.

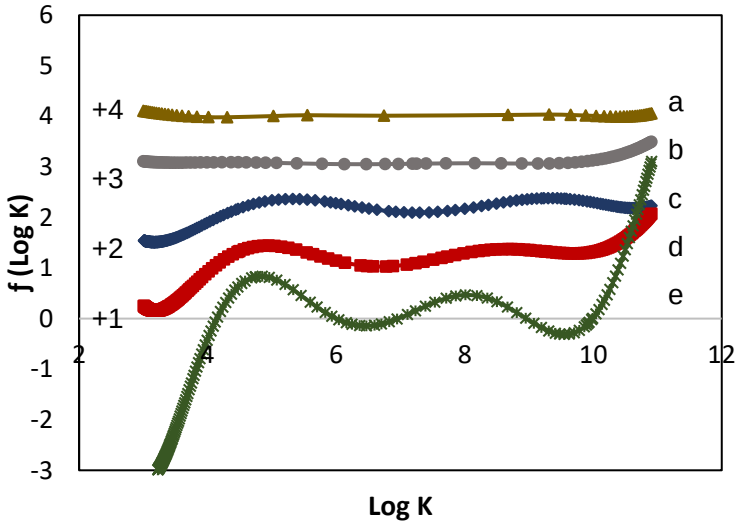

Figure 8. Proton Affinity Distribution for (a) Ni/SiO_2, (b) Ni/Al_2O_3, (c) Ni/HY, (d) Ni/HY-M, and (e) Ni/HY-M* (from incipient wetness impregnation method).

Table 3 summarizes the physicochemical properties of the synthesized catalysts. Results showed that the efficiency of the impregnation by SEA was almost complete, since the final loading of nickel in all catalysts (except for the Ni/SiO_2 catalyst) was very close to the theoretical

loading used for the synthesis; i.e. 0.5 wt% (see Appendix F). The percentage of Ni for the Ni/SiO_2 catalyst could indicate that the surface of the support was saturated at a lower concentration of the dissolved nickel complex as the one predicted with our calculation. On the other hand, the fact that silica had the highest OH surface density suggests that its hydroxyls are at a close distance from each other hence probably promoting surface interactions that rapidly saturate them.

Table 3.
Physicochemical properties of the catalysts pelletized, ground and sieved.

Sample	SA_{BET} [$m^2 \bullet g^{-1}$]	SA_{Micro} [$m^2 \bullet g^{-1}$]	SA_{Meso} [$m^2 \bullet g^{-1}$]	PV_{NLDFT} [$m^3 \bullet g^{-1}$]	PZ_{NLDFT} [Å]	PZ_{BJH} [nm]	$\%W_{Ni}$‡	OH Density‡ [$OH \bullet nm^{-2}$]	C‡ [$mmol \bullet g^{-1}$]
Ni/SiO_2	19	4	15	0.08	14.2	11.0	0.26	<2.2	0.07
Ni/Al_2O_3	129	--	129	0.39	--	9.4	0.46	<3.8	0.81
Ni/HY	582	522	60	0.25	7.3	--	0.46	<0.9	1.24
Ni/HY-M	526	351	175	0.30	6.9	2.1	0.43	>1.0	1.25
Ni/HY-M*	--	--	--	--	--	--	0.50	>1.1	1.50

*From incipient wetness impregnation method.
‡Measured from catalysts powders.

3.3. Catalytic results

Results from the tests made with dibenzothiophene are first presented (Section 4.3.1), and, afterwards, results from the simultaneous hydrodesulfurization of DBT and hydrodenitrogenation of indole over Ni/HY-M follow (Section 4.3.2).

3.3.1. Dibenzothiophene HDS reactions. Figure 9(a-d) shows the evolution of the catalytic behavior with time on stream for each catalyst. The main reaction products were biphenyl (BP) and tetrahydro-DBT (THDBT). Other secondary products were found but they were neither identified nor quantified. In the case of the catalysts supported on the zeolites, these products were heavier than DBT and were assumed to be alkylated DBTs (see Appendix M). In general, the activity of the catalysts in the HDS of DBT followed the order: Ni/HY-M > Ni/HY-M* > Ni/HY > > $Ni/SiO_2 \approx Ni/Al_2O_3$. Consequently, the most active catalyst was Ni/HY-M. Its activity was ca. 18% higher than that of the parent Ni/HY-M* catalyst; i.e. the one synthesized by incipient wetness

impregnation. This indicates the superiority of SEA in front of conventional impregnation. Furthermore, the advantages provided by the generation of mesopores in the zeolite support are also evident and they do not depend on the type of metal. We may recall that Fu et al.

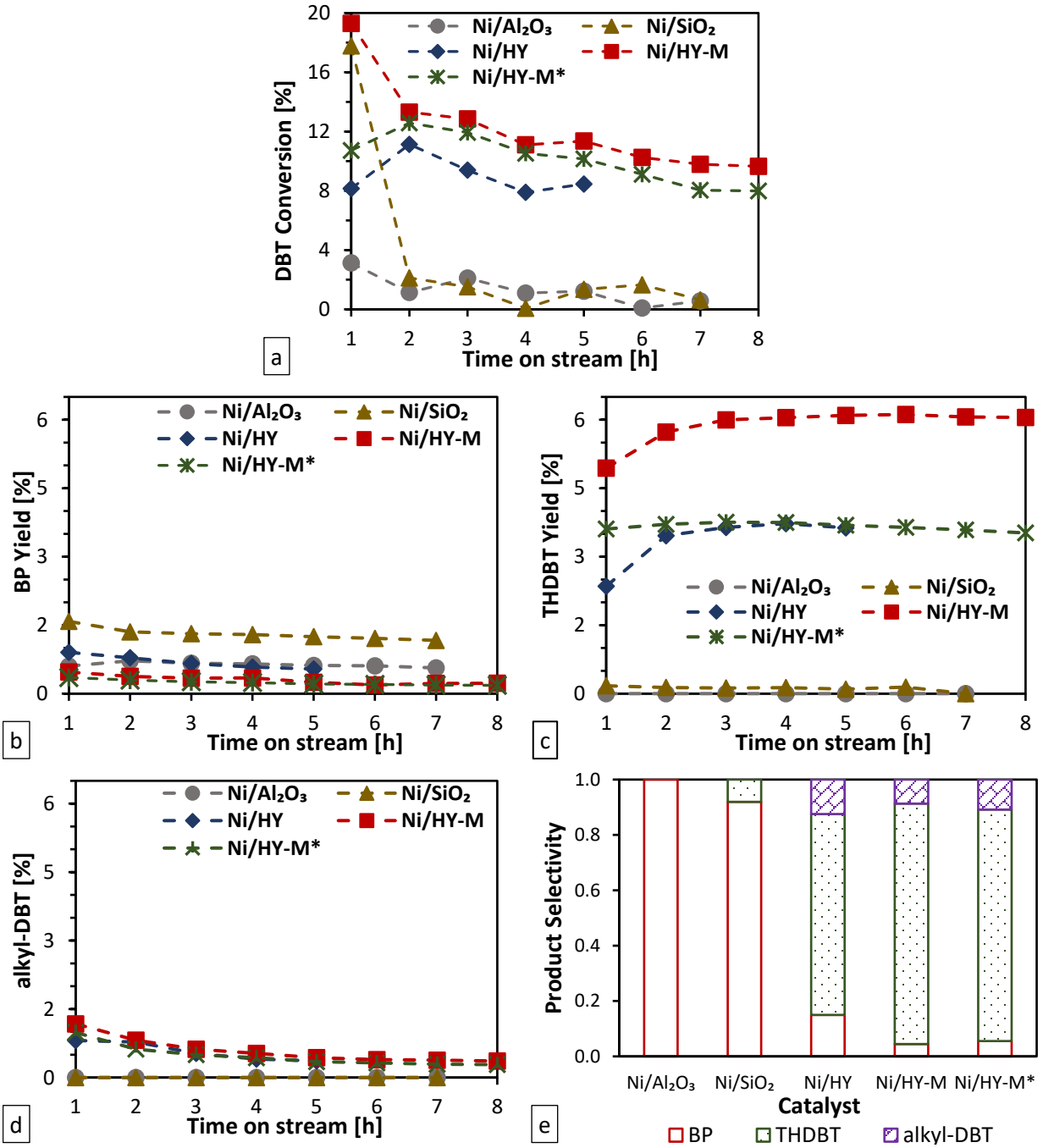

Figure 9. Activity versus Time on Stream from Each Catalyst (a) DBT Conversion, (b) BP Yield, (c) THDBT Yield and (d) alkyl-DBT Yield. (e) Average Product Selectivity for Each Catalyst. Carried out at 300°C and 5 MPa. *From incipient wetness impregnation method.

(Fu, et al., 2011) found a similar trend for Pd catalysts supported on a micro-mesoporous H-Y zeolite. The strong difference in catalytic performance between the catalysts supported on the zeolites and over SiO_2 and Al_2O_3 are due to the strong acidity of the former; particularly, their Brönsted acidity (Morales, Mora, Giraldo, & Centeno, 2011). Overall, our results prove that reduced monometallic nickel catalysts are active in HDS. Zhao et al. (Zhao, et al., 2019) earlier showed that alumina supported monometallic nickel is active for the hydrodesulfurization of thiophene; a molecule way more reactive than dibenzothiophene, at a much higher temperature, 370°C, than the one used in our study.

Figure 9e shows that the catalysts supported on SiO_2 and Al_2O_3 were mainly selective to the direct route of desulfurization. In contrast, the catalysts supported on the zeolites displayed a higher selectivity to the hydrogenation mediated route of HDS. This clearly shows an influence of the acidic characteristics of the supports on the selectivity of the reaction, alumina, with mainly Lewis acid sites promotes the DDS pathway and the Brönsted acid sites, found in the zeolites, promote HYD, as well as the cracking and further isomerization of DBT into alkyl-substituted DBTs (Isoda, Nagao, Ma, Korai, & Mochida, 1996; Kaneda, Wada, Murata, & Nomura, 1998; Isoda, Takase, Kusakabe, & Morooka, 2000).

3.3.1. Simultaneous HDS-HDN over Ni/HY-M. Under the reaction conditions used in this work, indole promoted the conversion of dibenzothiophene in the same way as Morales-Valencia found (Morales-Valencia E. M., 2019; Santiago Guerrero & Elder Bueno, 2019). In this case, the detected reaction products were biphenyl (BP), tetrahydro-DBT (THDBT), indoline (HIN), ortho-ethylcyclohexylalinine (OECHA), ortho-ethycyclohexylamine (OEA), and other cracking products (CP). Figure 10 summarizes the conversions and products yields for this reaction.

Indole promoted the conversion of DBT conversion by augmenting its conversion twice above the value obtained in the test without this compound. The yield of biphenyl was less than 0.5%, although the carbon balance of the reaction test suggests that this product was further cracked (see Appendix N). The absence of partially hydrogenated intermediates in the presence of indole suggests that this compound specifically promotes the DDS route of desulfurization. On the other hand, we found that indole was mostly converted into partially hydrogenated intermediates, therefore, HDN was not accomplished.

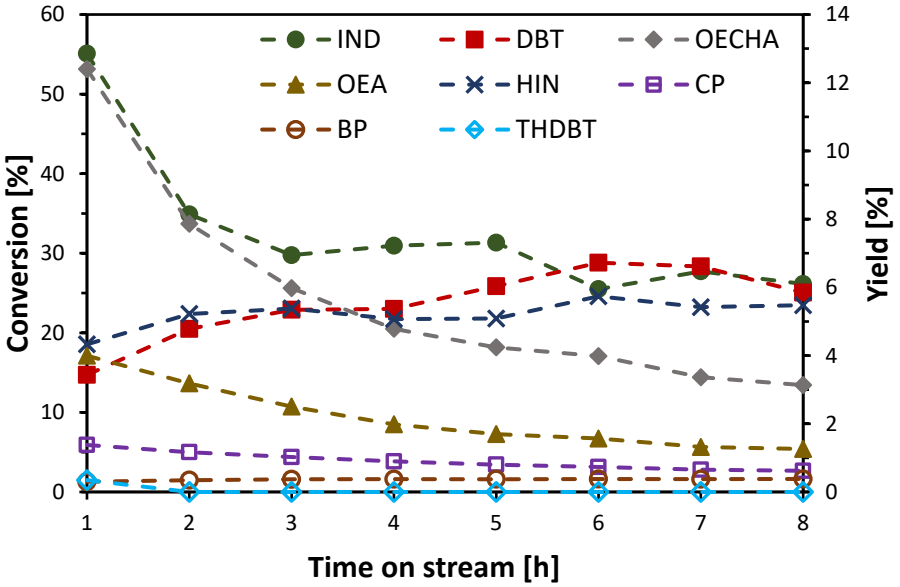

Figure 10. Conversion of DBT and IND, and Yield of OECHA, OEA, HIN, CP, BP, and, THDBT, in simultaneous HDS and HDN reactions carried out at 300°C and 5 MPa.

4. Conclusions

Several aluminosilicates were treated in order to be used as support of Ni in the synthesis of catalysts for hydrotreating. The textural properties and the acidity of the catalysts were determined, which were the most relevant physicochemical properties in the catalytic behavior for this work.

The catalytic behavior of supported Ni on SiO_2, Al_2O_3, HY zeolite, and, HY-M zeolite, was evaluated in hydrotreatment reactions. It was demonstrated that the micro-mesoporous zeolite

obtained the highest activity in the DBT conversion and it was found that the HDS of DBT over this zeolite was promoted by the presence of a nitrogenous compound, making the conversion increase to values of about double.

The evidence collected in this work suggests that the high activity of the catalysts supported on zeolites may be caused by the presence of Brönsted acid sites. Another finding in this work is that the incorporation of mesopores in the Y zeolite could improve the diffusion of the reagents to the catalytic sites, helping to increase the catalytic activity.

References

Abendroth, R. P. (1970, December). Behavior of a pyrogenic silica in simple electrolytes. *Journal of Colloid and Interface Science, 34*(4), 591-596. doi:10.1016/0021-9797(70)90223-7

Adkins, H., & Cramer, H. I. (1930, November). THE USE OF NICKEL AS A CATALYST FOR HYDROGENATION. *Journal of the American Chemical Society, 52*(11), 4349–4358. doi:10.1021/ja01374a023

Alboudwarej, H., Felix, J., Taylos, S., Badry, R., Bremner, C., Skeates, C., . . . Koerner, K. (2006, October 01). *La importancia del petróleo: Oilfield Review*. Retrieved November 18, 2018, from Schlumberger Web site: https://www.slb.com/resources/publications/industry_articles/oilfield_review/2006/or2006_sp_aut03_petroleopesado.aspx

Álvarez, M. C., Hoyos, L. J., & Zambrano, L. G. (2012, July 14). Modelado del proceso de hidrotratamiento de diésel. *Revista ION, XXV*(2), 7-14. Retrieved November 27, 2018

Arias, C. J., & Lozano, A. M. (2008). Comportamiento del catalizador CoMo/γ-Al2O3 modificado con boro, en reacciones silmutáneas de hidrogenación de oleofinas e hidrodesulfuración del 2-metil-tiofeno (Tesis de pregrado). Bucaramanga, Colombia: Universidad Industrial de Santander. Retrieved Noviembre 27, 2019

Baird, R., Eaton, A. D., Rice, E. W., Bridgewater, L., Association, A. W., & Federation, W. E. (2017). *Standard methods for the examination of water and wastewater* (23rd ed.). Washington, DC: American Public Health Association. Retrieved January 10, 2020

Baldovino-Medrano, V. G., Eloy, P., Gaigneaux, E., Giraldo, S. A., & Centeno, A. (2009, Octubre 25). Development of the HYD route of hydrodesulfurization of dibenzothiophenes over

Pd–Pt/γ-Al2O3 catalysts. *Journal of Catalysis, 267*(2), 129-139. doi:https://doi.org/10.1016/j.jcat.2009.08.004

Baldovino-Medrano, V. G., Giraldo, S. A., & Centeno, A. (2009). Behavior of PtMo/g−Al2O3−B2O3 Catalysts in Naphthalene Hydrodearomatization and Dibenzothiophene Hydrodesulfurization Reactions. *Información Tecnológica, 20*(6), 3-10. doi:10.4067/S0718-07642009000600002

Barbosa, A. L., Vega, A. F., & Amador, E. d. (2014, April 05). Hidrodesulfuración de crudos de petróleo: Base para el mejoramiento de combustibles. Una revisión. *Avances en Ciencias e Ingenierías, 5*(3), 37-60. Retrieved October 15, 2018, from http://www.exeedu.com/publishing.cl/av_cienc_ing/2014/Vol1/Nro3/3-ACI1190-13-full.pdf

Barrett, E. P., Joyner, L. G., & Halenda, P. p. (1951, January 01). The Determination of Pore Volume and Area Distributions in Porous Substances. I. Computations from Nitrogen Isotherms. *Journal of the American Chemical Society, 73*(1), 373-380. doi:10.1021/ja01145a126

Bataille, F., Lemberton, J.-L., Michaud, P., Pérot, G., Vrinat, M., Lemaire, M., . . . Breysse, M. K. (2000, April 25). Alkyldibenzothiophenes Hydrodesulfurization-Promoter Effect, Reactivity, and Reaction Mechanism. *Journal of Catalysis, 191*(2), 409-422. doi:10.1006/jcat.1999.2790

Beltrán, M. Á., & Sarmiento, W. R. (2008). Comportamiento de catalizadores PtMo soportados en alúmina modificada con boro en reacciones de hidrodeasromatización de naftaleno e hidrodesulfuración de dibenzotiofeno. Bucaramanga, Colombia: Universidad Industrial de Santander. Retrieved Noviembre 27, 2019

Borges, L. D., & Lemos de Macedo, J. (2016, December 1). Solid-state dealumination of zeolite Y: Structural characterization and acidity analysis by calorimetric measurements. *Microporous and Mesoporous Materials, 236*, 85-93. doi:10.1016/j.micromeso.2016.08.031

Breysse, M., Afanasiev, P., Geantet, C., & Vrinat, M. (2003, November). Overview of support effects in hydrotreating catalysts. *Catalysis Today, 86*(1-4), 5-16. doi:10.1016/S0920-5861(03)00400-0

Breysse, M., Geantet, C., Afanasiev, P., Blanchard, J., & Vrinat, M. (2008, January 15). Recent studies on the preparation, activation and design of active phases and supports of hydrotreating catalysts. *Catalysis Today, 130*(1), 3-13. doi:10.1016/j.cattod.2007.08.018

Broderick, D. H., & Gates, B. C. (1981, July). Hydrogenolysis and hydrogenation of dibenzothiophene catalyzed by sulfided CoO-MoO3/γ-Al2O3: The reaction kinetics. *AIChE Journal, 27*(4), 663-673. doi:10.1002/aic.690270419

Brunauer, S., Emmett, P. H., & Teller, E. (1938, february 01). Adsorption of Gases in Multimolecular Layers. *Journal of the American Chemical Society, 60*(2), 309-319. doi:10.1021/ja01269a023

Busca, G. (2017, December). Acidity and basicity of zeolites: A fundamental approach. *Microporous and Mesoporous Materials, 254*, 3-16. doi:10.1016/j.micromeso.2017.04.007

Chen, L.-H., Li, X.-Y., Rooke, J. C., Zhang, Y.-H., Tang, X.-Y., Tang, Y., . . . Su, B.-L. (2012). Hierarchically structured zeolites: synthesis, mass transport propierties and applications. *Journal of Materials Chemistry, XXII*(34), 17381-17403. doi: 10.1039/c2jm31957h

Chianelli, R. R. (2006). Periodic Trends Transition Metal Sulfide Catalysis: Intuition and Theory. *Oil & Gas Science and Technology, 61*(4), 503-513. Retrieved January 30, 2020, from https://ogst.ifpenergiesnouvelles.fr/articles/ogst/pdf/2006/04/ogst06008.pdf

Cho, H.-R. (2013). *The Rational Synthesis of Supported Noble Single or Bimetallic Catalysts by Strong ElectrostaticAdsorption.* South Carolina: U. South Carolina. Retrieved January 09, 2020, from https://scholarcommons.sc.edu/cgi/viewcontent.cgi?article=3531&context=etd

Cho, H.-R., & Regalbuto, J. R. (2015, May). The rational synthesis of Pt-Pd bimetallic catalysts by electrostatic adsorption. *Catalysis Today, 246*, 143-153. doi:10.1016/j.cattod.2014.09.029

Contescu, C., Contescu, A., & Schwarz, J. A. (1994, April 01). Thermodynamics of Proton Binding at the Alumina/Aqueous Solution Interface. A Phenomenological Approach. *The Journal of Physcal Chemistry, 98*(16), 4327-4335. doi:10.1021/j100067a020

Contescu, C., Jagiello, J., & Schwarz, J. A. (1993, April 26). Heterogeneity of Proton Binding Sites at the Oxide/Solution Interface. *Langmuir, 9*, 1754-1765. doi:10.1021/la00031a024

Contescu, C., Jagiello, J., & Schwarz, J. A. (1995). Proton Affinity Distributions: A Scientific Basis for the Design and Construction of Supported Metal Catalysts. *Studies in Surface Science and Catalysis, 91*, 237-252. doi:10.1016/S0167-2991(06)81760-X

Contescu, C., Popa, V., Miller, J., Ko, E., & Schwarz, J. (1995, November). Proton affinity distributions of TiO2-SiO2 and ZrO2-SiO2 mixed oxides and their relationship to catalyst activities for 1-butene isomerization. *Journal of Catalysis, 157*(1), 244-258. doi:10.1006/jcat.1995.1285

DANE. (2019). *Boletín Técnico de Exportaciones (EXPO) Octubre.* Departamento Administrativo Nacional de Estadísticas, Bogotá D.C. Retrieved January 03, 2020, from https://www.dane.gov.co/files/investigaciones/boletines/exportaciones/bol_exp_oct19.pdf

Das, M. R., Sahu, O. P., Borthakur, P. C., & Mahiuddin, S. (2004). Kinetics and adsorption behaviour of salicylate on a-alumina in aqueous medium. *Colloids and Surfaces A: Physicochemical and Engineering Aspects, 237*(1-3), 23–31. doi:10.1016/j.colsurfa.20

Dastanian, M., & Seyedeyn-Azad, F. (2010, October). Desulfurization of Gasoline over Nanoporous Nickel-Loaded Y-Type Zeolite atAmbient Conditions. *Industrial & Engineering Chemistry Research, 49*(22), 11254-11259. doi:10.1021/ie100941s

Deka, R. C. (1998, May). Acidity in zeolites and their characterization by different spectroscopic methods. *Indian Journal of Chemical Technology, 5*, 109-123. Retrieved January 24, 2020, from http://nopr.niscair.res.in/bitstream/123456789/30826/1/IJCT%205(3)%20109-123.pdf

Dias, N. L., & Ribeiro do Carmo, D. (2006). Adsorption at Silica, Alumina, and Related Surfaces. *Encyclopedia of Surface and Colloid Science, 1*, 209-228.

Ding, L., Zheng, Y., Zhang, Z., Ring, Z., & Chen, J. (2007, March 1). HDS, HDN, HDA, and hydrocracking of model compounds over Mo-Ni catalysts with various acidities. *Applied Catalysis A: General, 319*, 25-37. doi:10.1016/j.apcata.2006.11.016

Drobná, H., Kout, M., Sołtysek, A., González, V., Caballero, A., & Capek, L. (2017, Febrero 09). Analysis of Ni species formed on zeolites, mesoporous silica and alumina supports and their catalytic behavior in the dry reforming of methane. *Reaction Kinetics Mechanisms and Catalysis Journal, 121*(1), 255-274. doi:10.1007/s11144-017-1149-3

Duval, Y., Mielczarski, J. A., Pokrovsky, O. S., Mielczarski, E., & Ehrhardt, J. J. (2002, February 20). Evidence of the Existence of Three Types of Species at the Quartz−Aqueous Solution Interface at pH 0−10: XPS Surface Group Quantification and Surface Complexation Modeling. *The Journal of Physcal Chemistry, 106*(11), 2937-2945. doi:10.1021/jp012818s

Ecopetrol S.A. (2014, September 18). *Ecopetrol: Exportaciones*. Retrieved October 15, 2018, from Ecopetrol S.A. Portal: https://www.ecopetrol.com.co/wps/portal/es/ecopetrol-web/productos-y-servicios/comercio-internacional/exportaciones/exportaciones-de-crudo/

Egorova, M., & Prins, R. (2004, June 10). Competitive hydrodesulfurization of 4,6-dimethyldibenzothiophene, hydrodenitrogenation of 2-methylpyridine, and hydrogenation of naphthalene over sulfided NiMo/γ-Al2O3. *Journal of Catalysis, 224*(2), 278-287. doi:10.1016/j.jcat.2004.03.005

Egorova, M., & Prins, R. (2004, May 28). Hydrodesulfurization of dibenzothiophene and 4,6-dimethyldibenzothiophene over sulfided NiMo/γ-Al2O3, CoMo/γ-Al2O3, and Mo/γ-Al2O3. *Journal of Catalysis, 225*(2), 417-427. doi:10.1016/j.jcat.2004.05.002

Egorova, M., & Prins, R. (2004, February). Promotion Effect of 2-Methylpiperidine on the Direct Desulfurization of Dibenzothiophene over NiMo/γ-Al2O3. *Catalysis Letters, 92*(3-4), 87-91. doi:10.1023/B:CATL.0000014344.37981.9c

EPA. (2017, January 19). *Cirteria Air Pollutants*. (U. S. Governement, Editor, & Enviromental Protection Agency (EPA)) Retrieved January 03, 2020, from https://www.epa.gov/criteria-air-pollutants

Eri, S., Goodwin, J. G., Marcelin, G., & Riis, T. (1987, October 23). *United States Patent No. 4.801.573*. Retrieved January 10, 2020

Fan, Y. V., Perry, S., Klemeš, J. J., & Lee, C. T. (2018, May 21). A review on air emissions assessment: Transportation. *Journal of Cleaner Production, 194*, 673-684. doi:10.1016/j.jclepro.2018.05.151

Feliczak-Guzik, A. (2018, March 15). Hierarchical zeolites: Synthesis and catalytic properties. *Microporous and Mesoporous Materials, 259*, 33-45. doi:10.1016/j.micromeso.2017.09.030

Fiol, N., & Villaescusa, I. (2009, February 13). Determination of sorbent point zero charge: usefulness in sorption studies. *Environmental Chemistry Letters, 7*(1), 79-84. doi:10.1007/s10311-008-0139-0

Fu, W., Zhang, L., Tang, T., Ke, Q., Wang, S., Hu, J., . . . Xiao, F.-S. (2011, September 13). Extraordinarily High Activity in the Hydrodesulfurization of 4,6-Dimethyldibenzothiophene over Pd Supported on Mesoporous Zeolite Y. *Journal of the American Chemical Society, 133*(39), 15346-15349. doi:10.1021/ja2072719

Furimsky, E., & Massith, F. E. (1999, Septiembre 27). Deactivation of hydroprocessing catalysts. *Catalysis Today, 52*(4), 381-495. doi:doi.org/10.1016/S0920-5861(99)00096-6

Gackowski, M., Tarach, K., Kuterasiński, Ł., Podobiński, J., Jarczewski, S., Kuśtrowski, P., & Datka, J. (2018, June). Hierarchical zeolites Y obtained by desilication: Porosity, acidity and catalytic properties. *Microporous and Mesoporous Materials, 263*, 282-288. doi:10.1016/j.micromeso.2017.11.051

García-Gutiérrez, J. L., Laredo, G. C., Fuentes, G. A., García-Gutiérrez, P., & Jiménez-Cruz, F. (2014, December 15). Effect of nitrogen compounds in the hydrodesulfurization of straight-run gas oil using a CoMoP/g-Al2O3 catalyst. *Fuel, 138*, 98-103. doi:10.1016/j.fuel.2014.08.008

García-Martínez, J., Johnson, M., Valla, J., Li, K., & Ying, J. Y. (2012, January 11). Mesostructured zeolite Y—high hydrothermal stability and superior FCC catalytic performance. *Catalysis Science & Technology, 2*(5), 987-994. doi:10.1039/c2cy00309k

Garnica, M. M. (2016). Estudio computacional de la inhibición de compuestos nitrogenados en la adsorción de compuestos poliaromáticos sobre una zeolita (Bachaelor Thesis). Bucaramanga, Colombia: Universidad Industrial de Santander.

Gary, J. H., Handwerk, G. E., & Kaiser, M. J. (2007). *PETROLEUM REFINING: Technology and Economics* (Fifth ed.). New York, United States of America: Taylor & Francis Group.

Glacier RIG. (2020, January 28). *InvestmentMine*. (MINING.COM) Retrieved January 29, 2020, from http://www.infomine.com/investment/metal-prices/

Gran, G. (1952, November). Determination of the equivalence point in potentiometric titrations. Part II. *The Analyst, 77*(920), 661-671. doi:doi.org/10.1039/AN9527700661

Grau, A. (2016). Preparación y caracterización de zeolitas jerarquizadas con estructura MFI y faujasita: Análisis de diferentes métodos de incorporación de mesoporosidad en las mismas (Tesis de doctorado). Alicante: Universidad de Alicante.

GREENWOOD, N., & EARNSHAW, A. (1997). Nickel, Palladium and Platinum. In N. GREENWOOD, & A. EARNSHAW, *Chemistry of the elements* (pp. 1144-1172). Butterworth-Heinemann. doi:10.1016/C2009-0-30414-6

Greenwood, R. (2003). Review of the measurement of zeta potentials in concentrated aqueous suspensions using electroacoustics. *Advances in Colloid and Interface Science, 106*(1-3), 55–81. doi:10.1016/s0001-8686(03)00105-2

Groen, J. C., Jansen, J. C., Moulijn, J. A., & Pérez, J. (2004, August 07). Optimal Aluminum-Assisted Mesoporosity Development in MFI Zeolites by Desilication. *The Journal of Physical Chemestry, 108*(35), 13062-13065. doi:10.1021/jp047194f

Huirache-Acuña, R., Gabriel Alonso-Nuñez, E. M., Rivera-Muñoz, G. O., & Pawelec, B. (2016). Trimetallic Sulfide Catalysts for Hydrodesulfurization. In *Applying Nanotechnology to the Desulfurization Process in Petroleum Engineering* (pp. 240-262). Hershey: IGI Global. doi:10.4018/978-1-4666-9545-0.ch008

Ingman, F., & Still, E. (1966, October). Graphic method for the determination of titration end-points. *Talanta, 13*(10), 1431-1442. doi:10.1016/0039-9140(66)80084-X

Isoda, T., Nagao, S., Ma, X., Korai, Y., & Mochida, I. (1996, September 19). Hydrodesulfurization Pathway of4,6-Dimethyldibenzothiophene through Isomerizationover Y-Zeolite Containing CoMo/Al2O3Catalyst. *Energy & Fuels, 10*(5), 1078-1082. doi:10.1021/ef960048r

Isoda, T., Takase, Y., Kusakabe, K., & Morooka, S. (2000, April 27). Changes in Desulfurization Reactivity of4,6-Dimethyldibenzothiophene by Skeletal IsomerizationUsing a Ni-Supported Y-Type Zeolite. *Energy & Fuels, 14*(3), 585-590. doi:10.1021/ef990018z

Jaroniec, M., Kruk, M., Olivier, J. P., & Koch, S. (2000). A new method for the accurate pore size analysis of MCM-41 and other silica based mesoporous materials. *Studies in Surface Science and Catalysis, 128*, 71-80. doi:10.1016/S0167-2991(00)80010-5

Jiménez, F. Y. (2007). Estudio, modelamiento y simulación de los procesos simultáneos de hidrodesulfuración (HDS), hidrodesnitrogenación (HND) e hidrodesaromatización (HDA) en gasóleos de vacío (Tesis de doctorado). Bucaramanga, Colombia: Universidad Industrial de Santander. Retrieved November 27, 2018

Kabe, T., Ishihara, A., & Tajima, H. (1992, June 1). Hydrodesulfurization of Sulfur-Containing Polyaromatic Compounds in Light Oil. *Industrial and Engineering Chemistry Research, 31*(6), 1577-1580. doi:10.1021/ie00006a023

Kanda, Y., Kawanishi, K., Tsujino, T., Al-otaibi, A. M., & Uemichi, Y. (2018). Catalytic Activities of Noble Metal Phosphides for Hydrogenation and Hydrodesulfurization Reactions. *Catalysts, VIII*, 160-171. doi:10.3390/catal8040160

Kaneda, K., Wada, T., Murata, S., & Nomura, M. (1998, February 14). Hydrocracking of Dibenzothiophenes Catalyzed byPalladium- and Nickel-Coloaded Y-type Zeolite. *Energy & Fuels, 12*(2), 298-303. doi:10.1021/ef970123d

Knözinger, H., & Ratnasamy, P. (1978). Catalytic Aluminas: Surface Models and Characterization of Surface Sites. *Catalysis Reviews, 17*(1), 31-70. doi:10.1080/03602457808080878

Koltai, T., Macaud, M., Guevara, A., Schulz, E., Lemaire, M., Bacaud, R., & Vrinat, M. (2002). Comparative inhibiting effect of polycondensed aromatics and nitrogen compounds on the hydrodesulfurization of alkyldibenzothiophenes. *Applied Catalysis A: General, 231*(1-2), 253-261. doi:10.1016/S0926-860X(02)00063-7

Kosmulki, M. (2001). *Chemical Properties of Material Surfaces* (1st ed., Vol. 102). Boca Raton: CRC Press. Retrieved January 11th, 2020

Kosmulski, M. (2001). Evaluation of points of zero charge of aluminum oxide reported in the literature. *Prace Naukowe Instytutu Górnictwa Politechniki Wrocławskiej. Konferencje, 95*(31), 5-14. doi:bwmeta1.element.baztech-article-BPW5-0004-0036

Kosmulski, M. (2009). *Surface Charging and Points of Zero Charge* (First ed.). Boca Raton: CRC Press. doi:10.1201/9781420051896

LA Vopa, V., & Satterfield, C. N. (1988, April 2). Poisoning of thiophene hydrodesulfurization by nitrogen compounds. *Journal of Catalysis, 110*(2), 375-387. doi:10.1016/0021-9517(88)90328-4

Laredo, G. C., & Altamirano, E. D. (2003, April 10). Inhibition effects of nitrogen compounds on the hydrodesulfurization of dibenzothiophene: Part 2. *Applied Catalysis A: General, 243*(2), 207-214. doi:10.1016/S0926-860X(02)00321-6

Leonardo, Y., Álvarez, R., Ocanto, F., & Linares, C. F. (2011, March 29). Síntesis y caracterización de CoMo y NiMo/Celeste Ultramarino y su uso en la reacción de hidrodesulfuración de tiofeno. *Revista Latinoamericana de Metalurgia y Materiales, 31*(2), 161-167. Retrieved October 15, 2018, from http://rlmm.org/ojs/index.php/rlmm/article/download/100/138

LEXICOOL. (n.d.). *LEXICOOL: Glosario de términos usados en el sector energético.* Retrieved October 15, 2018, from LEXICOOL: Diccionarios, traducción y recursos lingüísticos: https://static.lexicool.com/dictionary/NL2OG99088.pdf

Ley 1205. (2008, July 15). *República de Colombia: Diario Oficial Leyes 1205 y 1208.* Retrieved November 27, 2018, from República de Colombia Diario Oficial: https://docs.colombia.justia.com/nacionales/leyes/ley-1208-de-2008.pdf

Liu, M., Ren, Y., Wu, J., Wang, Y., Chen, J., Lei, X., & Zhu, X. (2020, February). Effect of cations on the structure, physico-chemical properties and photocatalytic behaviors of silver-doped zeolite Y. *Microporous and Mesoporous Materials, 293,* 109800-109808. doi:10.1016/j.micromeso.2019.109800

López S., A. (2019, October 31). En 2020 habría menos pozos para producir petróleo y gas. *Portafolio*. Retrieved November 27, 2019, from https://www.portafolio.co/economia/en-2020-habria-menos-pozos-para-producir-petroleo-y-gas-535174

López, R. H. (2004). *Caracterización de Medios Porosos y Procesos Percolativos y de Transporte (PhD Thesis).* San Luis, Argentina: Universidad Nacional de San Luis. Retrieved January 12, 2020, from http://linux0.unsl.edu.ar/~rlopez/cap3new.pdf

Ma, X., Sakanishi, K., & Mochida, I. (1996, August). Hydrodesulfurization reactivities of various sulfur compounds in vacuum gas oil. *Industrial and Engineering Chemistry Research, 35*(8), 2487-2494. doi:10.1021/ie960137r

Macaud, M., Milenkovic, A., Schulz, E., Lemaire, M., & Vrinat, M. (2000, July 25). Hydrodesulfurization of Alkyldibenzothiophenes: Evidence of Highly Unreactive Aromatic Sulfur Compounds. *Journal of Catalysis, 193*(2), 255-263. doi:10.1006/jcat.2000.2897

Martín-Martínez, J. M. (1990). *Adsorción física de gases y vapores por carbones.* Alicante, España: Universitat d´Alacant / Universidad de Alicante. Retrieved from https://rua.ua.es/dspace/bitstream/10045/4291/6/adsorcion_fisica_4.pdf

Meriño, L. I., Centeno, A., & Giraldo, S. A. (2000, Abril 24). Influence of the activation conditions of bimetallic catalysts NM–Mo/γ-Al2O3 (NM=Pt, Pd and Ru) on the activity in HDT reactions. *Applied Catalysis A: General, 197*(1), 61-68. doi:https://doi.org/10.1016/S0926-860X(99)00533-5

MINMINAS, & UPME. (2016, December). *Proyección de demanda de combustibles líquidos en Colombia.* Retrieved November 27, 2019, from Unidad de Planeación Minero Energética (UPME) Sitio Web:

http://www1.upme.gov.co/DemandaEnergetica/Proyeccio%CC%81nDemandaL%C3%ADquidos-Rev2016.pdf

Moosavi, E. S., Dastgheib, S. A., & Karimzadeh, R. (2012, October 23). Adsorption of Thiophenic Compounds from Model Diesel Fuel Using Copper and Nickel Impregnated Activated Carbons. *Energies, 5*(12), 4233-4250. doi:10.3390/en5104233

Morales, E. M., Mora, I. D., Giraldo, S. A., & Centeno, A. (2011, June). EFECTO DE LA PRESENCIA DE CLORO EN CATALIZADORES Pd/γ-Al2O3 SOBRE LA REACCIÓN DE HIDRODESULFURACIÓN DE DIBENZOTIOFENO. *Revista ION*, *24*(1), 53-60. Retrieved January 09, 2020, from http://www.scielo.org.co/pdf/rion/v24n1/v24n1a07.pdf

Morales-Valencia, E. M. (2019). *Analysis of inhibition effects on deep hydrodesulfurization using model reactions (PhD Thesis).* Bucaramanga, Colombia: Universidad Industrial de Santander. Retrieved January 10, 2020

Morales-Valencia, E. M., Castillo-Ariza, C. O., Giraldo, S. A., & Baldovino-Medrano, V. G. (2018, March 21). Kinetic Assessment of the Simultaneous Hydrodesulfurization of Dibenzothiophene and the Hydrogenation of Diverse Polyaromatic Structures. *ACS Catalysis*, *8*(5), 3926-3942. doi:10.1021/acscatal.8b00629

Nikulshin, P., Mozhaev, A., Lancelot, C., Blanchard, P., Payen, E., & Lamonier, C. (2016, October). Hydroprocessing catalysts based on transition metal sulfides prepared from Anderson and dimeric Co2Mo10-heteropolyanions. A review. *Comptes Rendus Chimie*, *19*(10), 1276-1285. doi:10.1016/j.crci.2015.10.006

Noh, J. S., & Schwarz, J. A. (1989). Estimation of the point of zero charge of simple oxides by mass titration. *Journal of Colloid and Interface Science, 130*(1), 157–164. doi:10.1016/0021-9797(89)90086-6

Ojeda-Niño, Ó. H., & Rincón-Ortiz, S. A. (2014). ANÁLISIS DE LA INFLUENCIA DE LA RELACIÓN Si/(Si+Al) EN LA REACTIVIDAD DE DIBENZOTIOFENO SOBRE CATALIZADORES Pd-Pt/Al2O3-SiO2 (Bachelor Thesis). Bucaramanga, Colombia: Universidad Industrial de Santander. Retrieved January 25, 2020

Okamoto, Y. (2008, January 25). A novel preparation-characterization technique of hydrosulfurization catalyst for cleaner fuels. *CATALYSIS TODAY, 132*, 9-17. doi:10.1016/j.cattod.2007.12.030

Park, J., & Regalbuto, J. R. (1995, October). A Simple, Accurate Determination of Oxide PZC and the Strong Buffering Effect of Oxide Surfaces at Incipient Wetness. *Journal of Colloid and Interface Science, 175*(1), 239-252. doi:10.1006/jcis.1995.1452

Pashai, M., Moghaddam, H. M., & Ghorbani, M. (2016, January 15). Point of zero charge of maghemite decorated multiwalled carbon nanotubes fabricated by chemical precipitation method. *Journal of Molecular Liquids, 216*, 117-125. doi:10.1016/j.molliq.2015.12.087

Pérez, D. J., Gaigneaux, E. M., Giraldo, S. A., & Centeno, A. (2011, Febrero 01). Interpretation of the catalytic functionalities of CoMo/ASA FCC-naphtha-HDT catalysts based on its acid properties. *Journal of Molecular Catalysis A: Chemical, 335*(1-2), 112-120. doi:https://doi.org/10.1016/j.molcata.2010.11.022

Pérez-Martínez, D. d., Acevedo-Quiroga, G. A., Giraldo-Duarte, S. A., & Centeno-Hurtado, A. (2011, January). Surface characterization of borated γ-alumina by using proton affinity distributions. *Revista Facultad de Ingeniería Universidad de Antioquia, 57*, 23-30. Retrieved January 09, 2020, from http://www.scielo.org.co/pdf/rfiua/n57/n57a03.pdf

Perez-Ramirez, J., Christensen, C. H., Egeblad, K., Christensen, C. H., & Groen, J. C. (2008, September 18). Hierarchical zeolites: enhanced utilisation of microporous crystals in

catalysis by advances in materials design. *Chemical Society Reviews, 37*(11), 2530-2542. doi:10.1039/B809030K

Project, D. o., Provost, U. D., Library, U. D., Program, C. S., & Merlot. (2019, August 18). *Chemestry LibreTexts: Overview of Reflux*. (L. Nichols, Editor) Retrieved January 08, 2020, from Chemestry LibreTexts: https://chem.libretexts.org/Bookshelves/Organic_Chemistry/Book%3A_Organic_Chemistry_Lab_Techniques_(Nichols)/1%3A_General_Techniques/1.3%3A_Heating_and_Cooling_Methods/1.3K%3A_Reflux

Ramérez-Corredores, M. M., & Borole, A. P. (2007). *Chapter 2 Conventional refining processes* (Vol. 164). Elsevier. doi:10.1016/S0167-2991(07)80242-4

Rana, M. S., Al-Barood, A., Brouresli, R., Al-Hendi, A. W., & Mustafa, N. (2018, August). Effect of organic nitrogen compounds on deep hydrodesulfurization of middle distillate. *Fuel Processing Technology¨, 177*, 170-178. doi:10.1016/j.fuproc.2018.04.014

Rangarajan, S., & Mavrikakis, M. (2016, April 7). DFT Insights into the Competitive Adsorption of Sulfur- and Nitrogen-Containing Compounds and Hydrocarbons on Co-Promoted Molybdenum Sulfide Catalysts. *ACS Catalysis, 6*(5), 2904-2917. doi:10.1021/acscatal.6b00058

Rangarajan, S., & Mavrikakis, M. (2017, December 4). On the Preferred Active Sites of Promoted MoS2 for Hydrodesulfurization with Minimal Organonitrogen Inhibition. *ACS Catalysis, 7*(1), 501-509. doi:10.1021/acscatal.6b02735

Regalbuto, J. (2006). *CATALYST PREPARATION - Science and Engineering* (1st ed.). Boca Raton: CRC Press. Retrieved January 09, 2020

Reinhoudt, H., Troost, R., van Schalkwijk, S., van Langeveld, A., Sie, S., van Veen, J., & Moulijn, J. (1999, Septiembre). Testing and characterisation of Pt/ASA for deep HDS reactions. *Fuel Processing Technology, 61*(1-2), 117-131. doi:https://doi.org/10.1016/S0378-3820(99)00034-X

Resolución 182087. (2007, December 17). *Ministerio de Minas y Energía: Memoria Resolución 182087*. Retrieved November 27, 2018, from Ministerio de Minas y Energías: https://www.minminas.gov.co/documents/10180/674559/memoria+t95+160620171.pdf/38d2eb3b-2de2-4a37-8e17-5949821f3c45

Restrepo-Garcia, J. R., Ramírez, G. E., & Baldovino-Medrano, V. G. (2018, February). Hydroprocessing of Phenanthrene Over Sulfided Fe–W Supported on Modified SBA-15. *Catalysis Letters , 148*, 621-641. doi:10.1007/s10562-017-2269-0

Rouquerol, J., Rouquerol, F., Llewellyn, P., Maurin, G., & Sing, K. (2013). *Adsorption by Powders and Porous Solids. Principles, Methodology and Applications* (2nd ed.). Academic Press. Retrieved January 12, 2020

Sachse, A., Grau-Atienza, A., Jardim, E. O., Linares, N., Thommes, M., & García-Martínez, J. (2017, July 17). Development of Intracrystalline Mesoporosity in Zeolites through Surfactant-Templating. *Crystal Growth and Design, 17*(8), 4289-4305. doi:10.1021/acs.cgd.7b00619

Santiago Guerrero, A. Y., & Elder Bueno, C. (2019). *Análisisde la Influencia del Indol sobre la Reacción de un Compuesto Refractario a la Hidrodesulfuración (Bachelor Thesis).* Bucaramanga, Colombia: Universidad Industrial de Santander. Retrieved January 26, 2020

Semana. (2019, December 14). ¿Cómo se moverá la economía en 2020?, en estos sectores está la clave. *Revista Semana*. Retrieved January 03, 2020, from

https://www.semana.com/economia/articulo/sectores-que-moveran-la-economia-colombiana-en-el-2020/644720

Shafi, R., & Hutchings, G. J. (2000, June 25). Hydrodesulfurization of hindered dibenzothiophenes: an overview. *Catalysis Today, 59*(3-4), 423-442. doi:doi.org/10.1016/S0920-5861(00)00308-4

Shcherban, N. D., Filonenko, S. M., Barakov, R. Y., Sergiienko, S. A., Yu, K., Heinmaa, I., . . . Murzin, D. Y. (2017). New insights in evaluation of acid sites in micro-mesoporous zeolite-likematerials using potentiometric titration method. *Applied Catalysis A, General, 543*, 34-42. doi:10.1016/j.apcata.2017.05.039

Song, C. (2003). An overview of new approaches to deep desulfurization for ultra-clean gasoline, diesel fuel and jet fuel. *Catalysis Today, 86*, 211-263. doi:10.1016/S0920-5861(03)00412-7

Tang, T., Zhang, L., Fu, W., Ma, Y., Xu, J., Jiang, J., . . . Xiao, F.-S. (2013, Julio 19). Design and Synthesis of Metal Sulfide Catalysts Supported on Zeolite Nanofiber Bundles with Unprecedented Hydrodesulfurization Activities. *Journal of the Amerincan Chemical Society, 135*(31), 11437-11440. doi:10.1021/ja4043388

Tao, X., Zhou, Y., Wei, Q., Ding, S., Zhou, W., Liu, T., & Li, X. (2017, January 15). Inhibiting effects of nitrogen compounds on deep hydrodesulfurization of straight-run gas oil over a NiW/Al2O3 catalyst. *FUEL, 188*, 401-407. doi:10.1016/j.fuel.2016.09.055

Tavolaro, P., Tavolaro, A., & Martino, G. (2009, April 1). Influence of zeolite PZC and pH on the immobilization of cytochrome c: A preliminary study regarding the preparation of new biomaterials. *Colloids and Surfaces B: Biointerfaces, 70*(1), 98-107. doi:10.1016/j.colsurfb.2008.12.019

Thommes, M., Kaneko, K., Neimark, A. V., Olivier, J. P., Rodriguez-Reinoso, F., Rouquerol, J., & Sing, K. S. (2015, August 02). Physisorption of gases, with special reference to the evaluation of surface area and pore size distribution (IUPAC Technical Report). *Pure and Applied Chemistry, 87*(9-10), 1051-1069. doi:10.1515/pac-2014-1117

Trueba, M., & Trasatti, S. P. (2005). g-Alumina as a Support for Catalysts: A Review of Fundamental Aspects. *European Journal of Inorganic Chemistry, 17*, 3393–3403. doi:10.1002/ejic.200500348

Van Aelst, J., Verboekend, D., Philippaerts, A., Nuttens, N., Kurttepeli, M., Gobechiya, E., . . . Sels, B. F. (2015). Catalyst Design by NH4OH Treatment of USY Zeolite. *Advanced Functional Materials, XXV*(46), 7130-7144. doi:10.1002/adfm.201502772

Vázquez, I., López, A., Berhault, G., & Guevara, A. (2019, Enero 15). Effect of support on the acidity of NiMo/Al2O3-MgO and NiMo/TiO2-Al2O3 catalysts and on the resulting competitive hydrodesulfurization/hydrodenitrogenation reactions. *Fuel, 236*, 55-64. doi:10.1016/j.fuel.2018.08.053

Wang, Z.-G., Pei, J.-N., Chen, S.-L., Zhou, Z., Yuan, G.-M., Wang, Z.-Q., . . . Jiang, H.-J. (2017, Abril 05). The surface properties of aluminated meso–macroporous silica and its catalytic performance as hydrodesulfurization catalyst support. (X.-Q. Zhu, Ed.) *Petroleum Science, 14*(2), 424-433. doi:DOI 10.1007/s12182-017-0150-9

Westerman, D. W., RuffioM, I. E., Wainwright, S., & Foster, N. R. (1980, January 06). Chemical analysis of vanadium pentoxide catalysts. *Analytica Chimica Acta, 117*, 285-291. doi:10.1016/0003-2670(80)87028-0

Yáñez, E., Ramírez, A., Uribe, A., Castillo, E., & Faaij, A. (2018, March 01). Unravelling the potential of energy efficiency in the Colombian oil industry. *Journal of Cleaner Production, 176*, 604-628. doi:https://doi.org/10.1016/j.jclepro.2017.12.085

Yates, D. E., & Healy, T. W. (1976, April). The structure of the silica/electrolyte interface. *Journal of Colloid and Interface Science, 55*(1), 9-19. doi:10.1016/0021-9797(76)90003-5

Yocupicio, R. I., Díaz de León, J. N., Zepeda, T. A., & Fuentes, S. (2017, Enero 26). Study of CoMo catalysts supported on hierarchical mesoporous zeolites for hydrodesulfurization of dibenzothiophene. *Revista Mexicana de Ingeniería Química, 16*(2), 503-520. Retrieved Noviembre 27, 2019, from http://www.redalyc.org/pdf/620/62052087016.pdf

Yu, K., Kumar, N., Aho, A., Roine, J., Heinmaa, I., Murzin, D. Y., & Ivaska, A. (2016, January 18). Determination of acid sites in porous aluminosilicate solid catalysts foraqueous phase reactions using potentiometric titration method. *Journal of Catalysis, 335*, 117-124. doi:10.1016/j.jcat.2015.12.010

Zeuthen, P., Knudsen, K. G., & Whitehurst, D. (2001, February 20). Organic nitrogen compounds in gas oil blends, their hydrotreated products and the importance to hydrotreatment. *Catalysis Today, 65*(2-4), 307-314. doi:10.1016/S0920-5861(00)00566-6

Zhang, R., Xu, S., Raja, D., Khusni, N. B., Liu, J., Zhang, J., . . . Fan, X. (2019, April). On the effect of mesoporosity of FAU Y zeolites in the liquid-phase catalysis. *Microporous and Mesoporous Materials, 278*, 297-306. doi:10.1016/j.micromeso.2018.12.003

Zhao, J., Chai, Y., Liu, B., Liu, Y., Liu, Y., & Liu, C. (2019, Enero 10). The effect of hydrogen on thiophene catalytic removal over Ni/Al2O3. *Catalysis Comminucations, 119*, 6-10. doi:https://doi.org/10.1016/j.catcom.2018.10.007

Appendix

Appendix A. Elimination of Na and Cl from silica support.

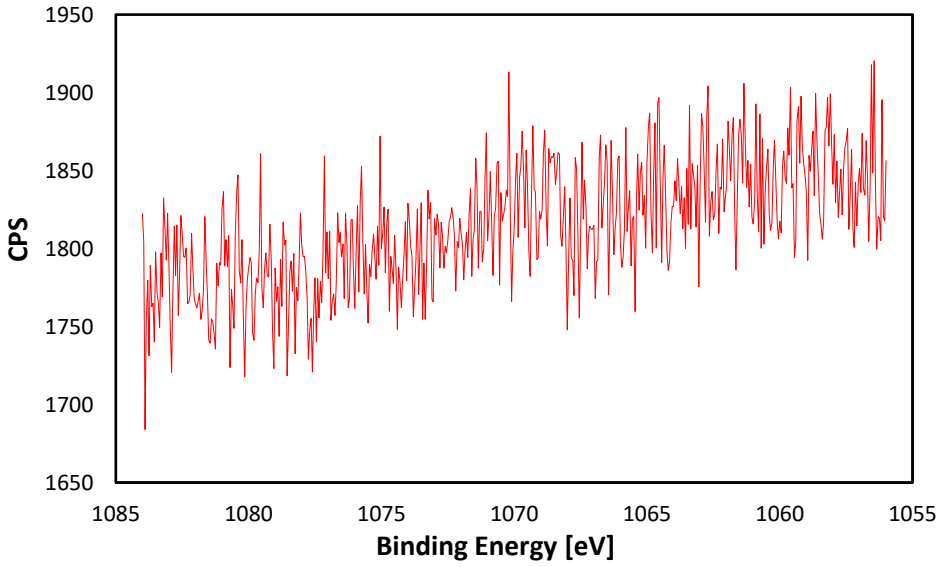

Figure A.1. High-resolution XPS spectrum of the Na 1s region for silica after acid treatment in order to Na removal.

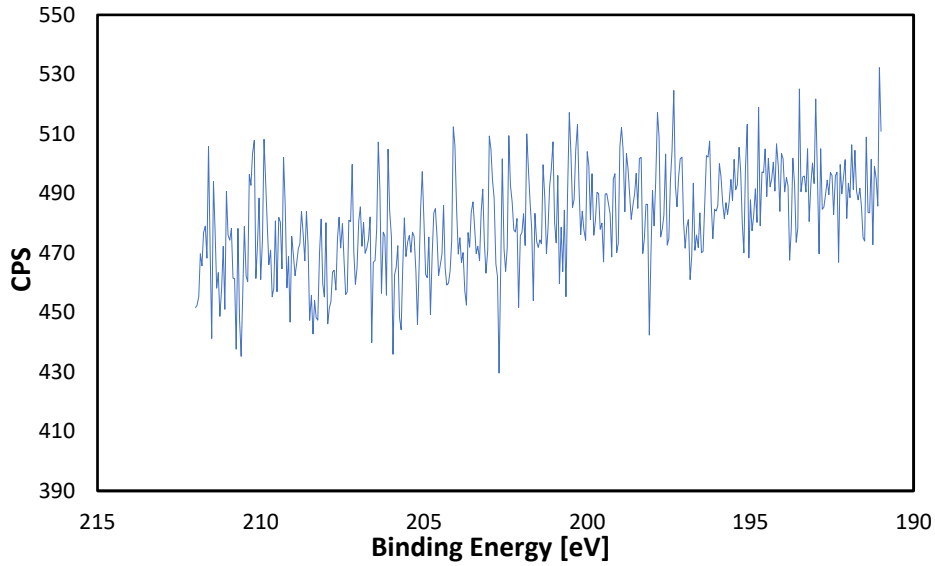

Figure A.2. High-resolution XPS spectrum of the Cl 2p region for silica after acid treatment in order to Na removal.

Appendix B. Conditions for the generation mesoporous from NaY zeolite.

To define the better conditions in order to obtain the micro and mesoporous zeolite, two criteria were established, the first is that the ratio between mesoporous surface area and microporous surface area to be greater than 0.5 and that to be smaller than 1.0, and the other, that the ratio between mesoporous volume and microporous volume to be greater than 1.0 and that to be smaller than 2.0. In Table B, is summarized all the conditions and zeolites evaluated.

Table B.1.
Summary of the conditions and zeolites evaluated to obtain micro and mesoporous simultaneously.

Zeolite	$[C_6H_8O_7]$ [M]	[NaOH][M]	Temperature [°C]	Time [h]	Ratio SA_{Meso}/SA_{Micro}	Ratio V_{Meso}/V_{Micro}
Mordenite	--	0.001	150	15	*	*
		0.050				
		0.100				
		0.300			3.5	77.3
		0.400			7.1	-1481.5
		0.500			3.5	223.2
NaY	0.10	0.025	150	15	0.6	1.2
		0.050	150	15	0.2	0.6
			206	15	0.3	1.1
				24	0.3	1.1
		0.100	150	15	0.2	0.5
			206		0.2	0.6
		0.150	150	15	0.1	0.3
		0.200			0.1	0.4
		0.250			0.1	0.2
	0.21	0.100	150	15	0.2	0.4
			206		12.5	-94.7

*The physisorption analysis never ended and the results were not conclusive.

Appendix C. Calculations for the impregnation of Ni in the supports.

In order to synthesize each of the catalysts, the following calculations were realized:

$$W_{PS} = \frac{W_M}{\%P_{PS}} * \frac{MW_{PS}}{MW_M} \quad \text{Eq. C1}$$

Where,

W_{PS} and W_M are the weight of the precursor salt and of the metal, respectively.
MW_{PS} and MW_M are the molecular weight of the precursor salt and the metal.
$\%P_{PS}$ is the purity percent of the precursor salt.

$$W_M = W_S * \frac{\%W_M}{(1 - \%W_M)} \quad \text{Eq. C2}$$

Where,

W_S is the weight of the support.
$\%W_M$ is the Weight percent of the metal.

$$V_w = 6 * W_S * PV_S \quad \text{Eq. C3}$$

Where,

V_W is the volume of the water necessary.
PV_S is the pore volume of the support.

$$W_{AS} = RM * MW_{AS} * \frac{W_M}{MW_M} \quad \text{Eq. C4}$$

Where,

W_{AS} is the weight of the ammoniacal solution.
RM is the molar ratio between the ammonia and the nickel.
MW_{AS} is the molecular weight of the ammoniacal solution.

The following chemical reactions occur during metal impregnation:

$$Ni^{2+}(aq) + 2NH_3(aq) + 2H_2O(l) \leftrightarrow Ni(OH)_2(s) + 2NH_4^+(aq) \quad \text{Eq. C5}$$

$$Ni(OH)_2(s) + 6NH_3(aq) \leftrightarrow [Ni(NH_3)_6]^{2+} + 2OH(aq) \quad \text{Eq. C6}$$

Starting from the moles of nickel nitrate hexahydrate added, the necessary moles of ammonium hydroxide are calculated to obtain only the complex ion $[Ni(NH_3)_6]^{2+}$, therefore, according to reactions Eq. C5 and Eq. C6 8 moles of ammonia per mole of nickel are required, that is RM.

$$V_{AS} = \frac{W_{AS}}{\%P_{AS} * \rho_{AS}} \quad \text{Eq. C7}$$

Where,

V_{AS} is the volume of the ammoniacal solution necessary.
$\%P_{AS}$ is the purity percent of the ammoniacal solution.
ρ_{AS} is the density of the ammoniacal solution.

Appendix D. Volume and pore size distribution for the supports.

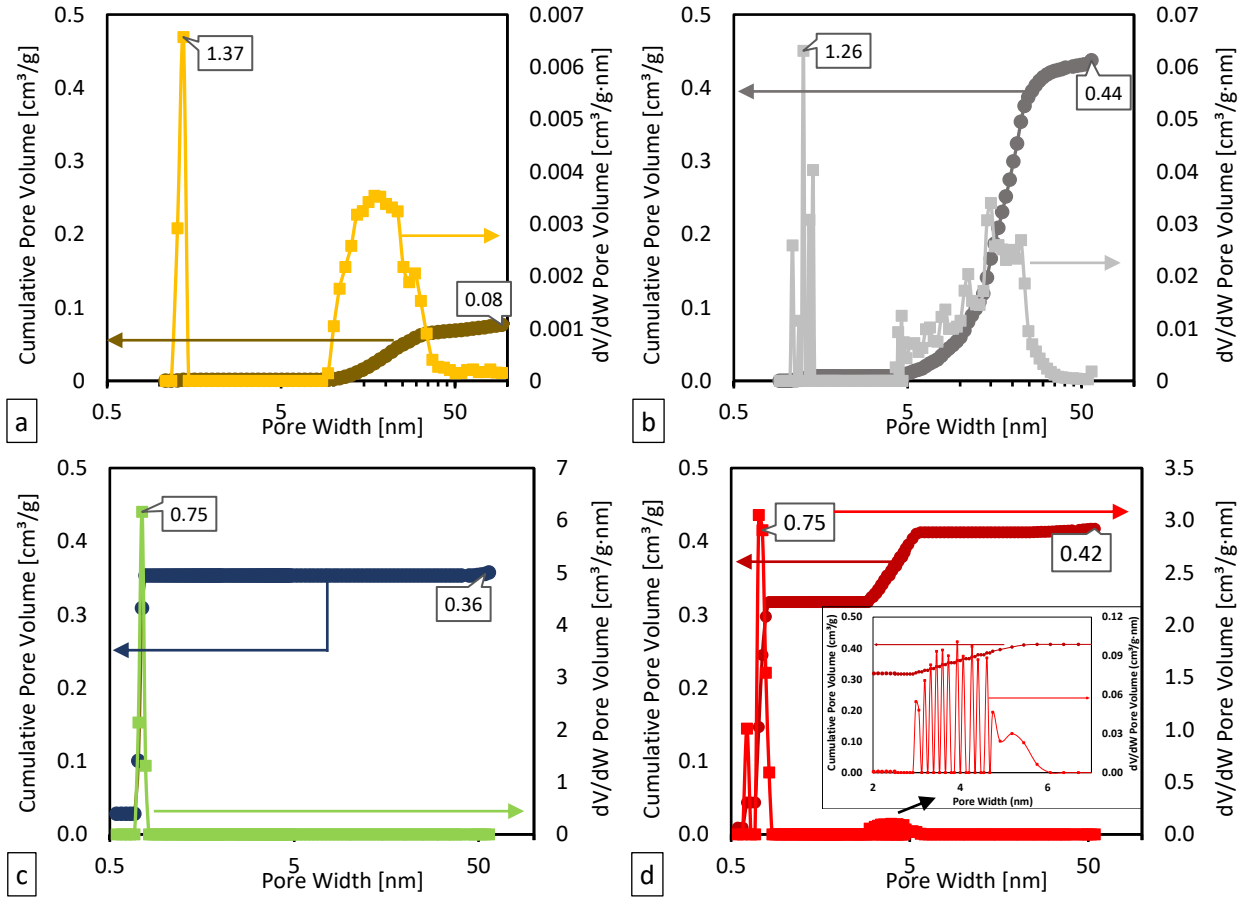

Figure D1. Volume and size pore calculated by NLDFT method for (a) SiO_2, (b) Al_2O_3, (c) HY, and, (d) HY-M.

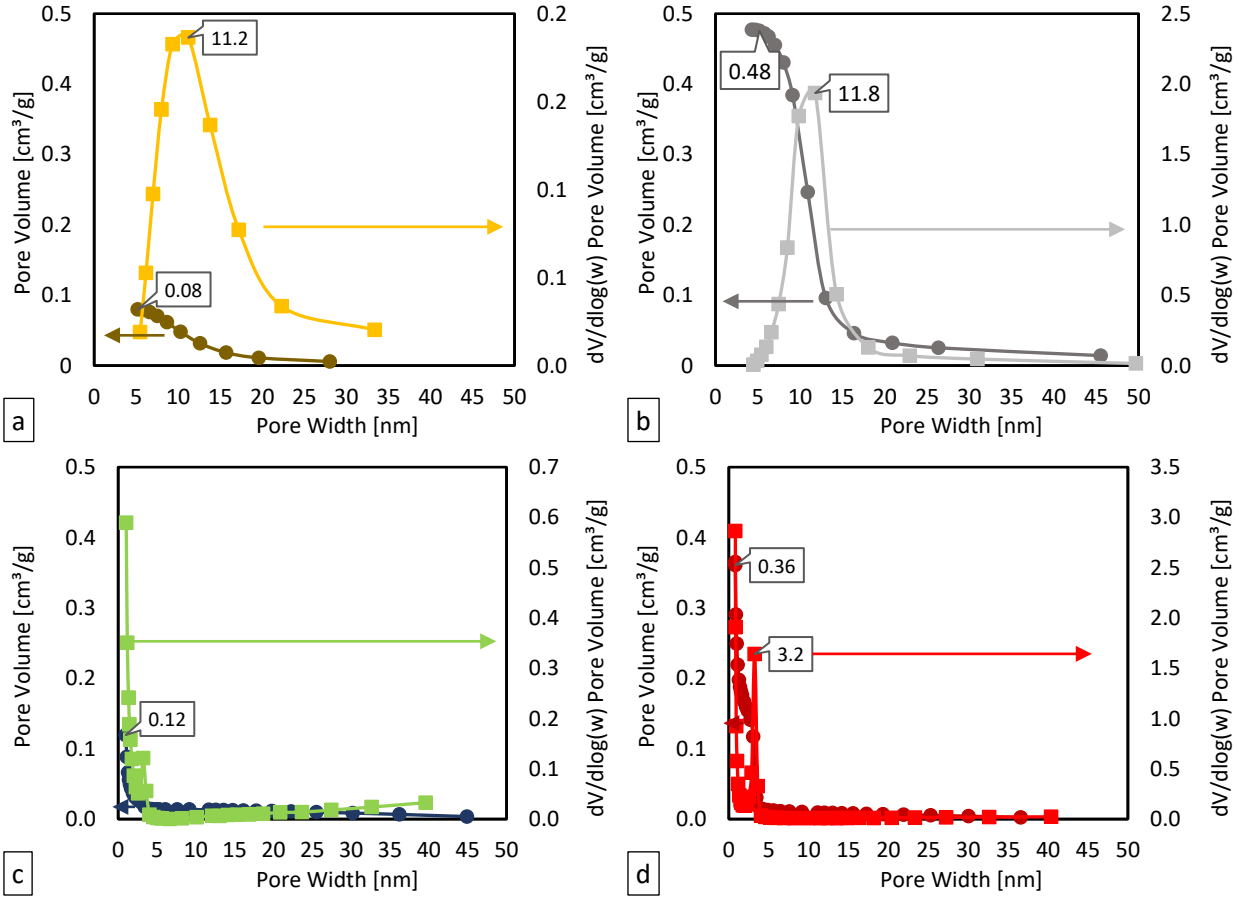

Figure D2. Volume and size pore calculated by BJH method for (a) SiO_2, (b) Al_2O_3, (c) HY, and, (d) HY-M.

Appendix E. Procedures for calculating OH surface groups from each material.

Appendix E.1. For de alumina. The location and quantification of the peaks corresponding to each OH group, according to the ranges reported in the literature (Table E1), was performed with the help of specialized software (*Fityk V.1.3.1*) for the analysis of curves. Once the peaks were located, a deconvolution of the overlapping ones was performed, using gauss curves. The Gaussian curves were the ones that best adapted to the data to find the convergence of the system with minimal error with respect to the original data. The quantification of each of the types of OH sites was made using the area under the curve of each of the peaks present in the proton affinity distribution (Contescu, Popa, Miller, Ko, & Schwarz, 1995).

Table E.1.1.
pH range for the OH sites present on the surface of the γ-Al_2O_3 (Contescu, Jagiello, & Schwarz, 1995; Contescu, Jagiello, & Schwarz, 1993).

Type of site	Range of pH
III	2.0 < pH < 3.5
IIA	3.5 < pH < 5.5
IIB	pH < 2.0; pH > 12.0
IA	5.5 < pH < 9.5
IB	9.5 < pH < 12.0

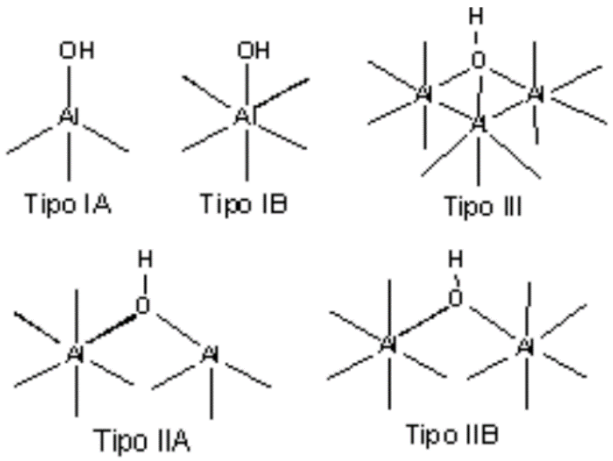

Figure E.1.1. Surface models and configuration of OH sites for Al2O3. Taken of (Knözinger & Ratnasamy, 1978).

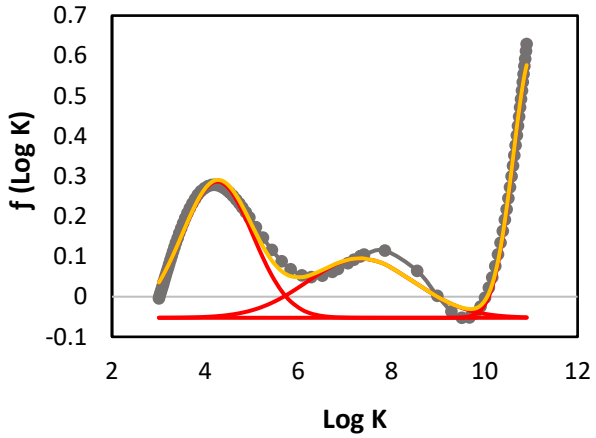

Figure E.1.2. Proton affinity distribution as a function of pH for Al_2O_3 and peak decomposition.

Table E.1.2.

Quantification of the concentration of OH groups depending of the type of site for Al_2O_3.

Support	**C [mmolH^+•g^{-1} of support]**		
	IIA	IA	IB
Al_2O_3	0.650	0.434	0.697

Appendix E.2. For the silica. The quantification of the silanol groups was calculated using the volume of the base added until reach a pH value of about 8.5, according to the following equation:

$$C_{(OH)} = \frac{V_B * [B.C]}{W_S} \qquad \text{Eq. E.2.1}$$

Where,

$C_{(OH)}$ is the concentration of the silanol groups.
V_B is the volume of the base added.
$[B.C]$ is the base concentration.
W_S is the weight of the support in the titration.

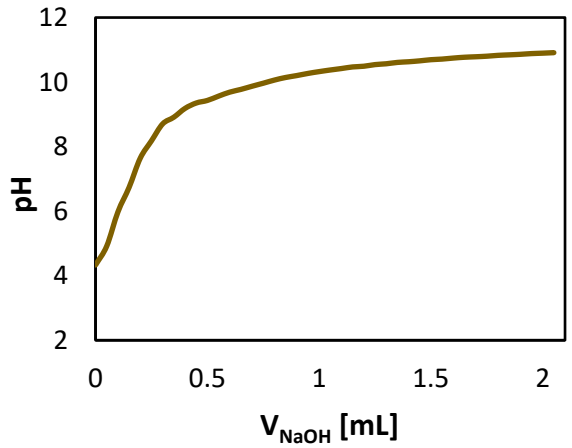

Figure E2.1. Titration of silica using a strong base (NaOH) in order to calculate the concentration of silanol groups.

Appendix E.3. For the zeolites. The Gran method was selected for the data analysis (Gran, 1952). The common sigmoidal potentiometric titration curve is transformed into a linear form with the Gran function, which allows calculation of the equivalence volume by a standard linear regression method using several points on the titration curve (Yu, et al., 2016). Ingman and Still have derived a more accurate Equation than (Eq. E.3.8.) to describe the titration of a weak acid with a strong base (Ingman & Still, 1966).

When a weak acid (HR) is titrated with a strong base the following reaction takes place:

$$HR + OH^- \rightarrow R^- + H_2O \qquad \text{Eq. E.3.1.}$$

The acid takes also part in the following equilibrium:

$$HR \rightleftharpoons H^+ + R^- \qquad \text{Eq. E.3.2.}$$

with the protonation constant:

$$K = \frac{[HR]}{[H^+] \cdot [R^-]} \qquad \text{Eq. E.3.3.}$$

The total concentration of the acid, C_{HR}, is:

$$C_{HR} = [HR] + [R^-] \qquad \text{Eq. E.3.4.}$$

The following mass balance is valid at each titration point:

$$V_0 C_{HR} = (V_0 + V) \cdot ([HR] + [R^-]) \qquad \text{Eq. E.3.5.}$$

The initial concentration of the acid is V_0, the volume of added base is V and according to reaction (Eq. E.3.1.) the following equation can be written after each addition of the strong base:

$$V \cdot C_{OH} = (V_0 + V) \cdot [R^-] \qquad \text{Eq. E.3.6.}$$

C_{OH} is the base concentration. If the consumption of the strong base at the equivalence point is denoted by V_{eq} the following equation is valid at the equivalence point

$$V_0 \cdot C_{HR} = V_{eq} \cdot C_{OH} \qquad \text{Eq. E.3.7.}$$

Combination of Equations E.3.3., E.3.5., E.3.6. and E.3.7. gives:

$$V_{eq} - V = K \cdot [H^+] \cdot V \qquad \text{Eq. E.3.8.}$$

When the term $[H^+] \cdot V$ is plotted as a function of V a straight line is obtained and it intersects the V -axis at V_{eq}. The slope of the line is $\frac{1}{K}$. This method allows simultaneous determination of both V_{eq} and K.

Equation E.3.8. is valid so far, the acid HR does not take part in any other equilibrium reaction than Eq. E3.2. When the material, as zeolites in this study, having several acid groups with different strengths is titrated, the entire titration curve when processed with the Equation E.3.8. will consists of linear sections with different slopes, i.e., K. When one linear section is converted to the following some curvature will appear on the line. In the evaluation of the titration values for both $V_{eq}$and K, and for each equilibrium only the linear parts should be used (Yu, et al., 2016).

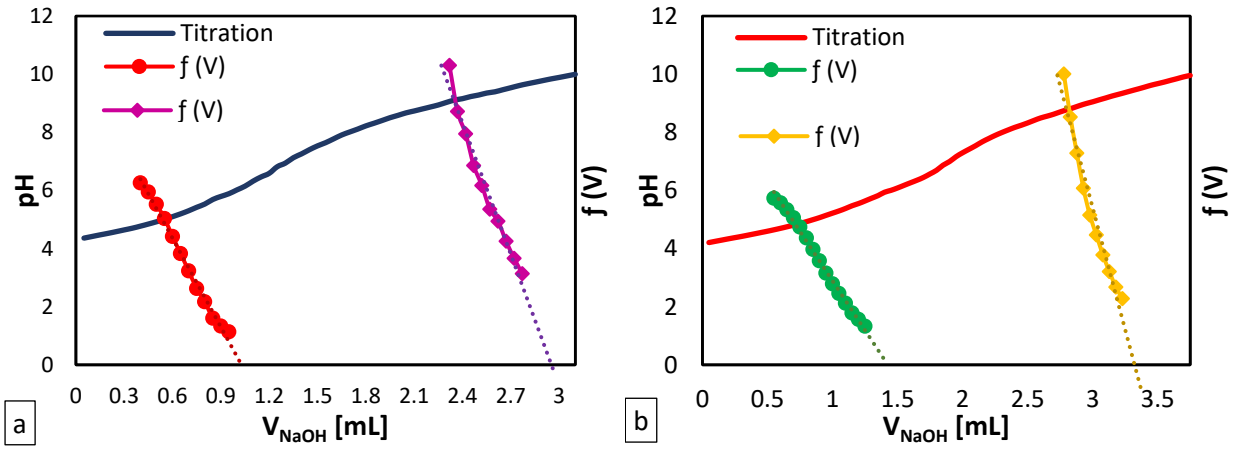

Figure E.3.1. Determination of the acid sites with the Gran method in titration of (a) HY zeolite, and, (b) HY-M zeolite. The points marked with circles (reds and greens) and diamonds (purples and yellows) are obtained by transforming the original titration data with the Gran f(V) (Eq. E.3.8.). The numerical scales for the different functions of f(V) are not shown.

Table E.3.1.
Quantification of the concentration of acid sites for HY and HY-M.

Support	C [mmolH$^+$•g^{-1} of support]	
	$R_1^-H^+$	$R_2^-H^+$
HY	0.503	0.839
HY-M	0.995	0.662

Appendix F. Calculations to obtain the maximum impregnation percent to each support.

Starting from the concentration of OH sites and the specific area, the maximum percentage of Ni impregnation is obtained, considering that the Ni/OH ratio is 1:2. As it is shown below.

$$N°OH_{av} = OH_d * SA_{BET} * W_S \quad \text{Eq. F.1.}$$

Where,

$N°OH_{av}$ is the number of the OH groups available on the support.
OH_d is the OH density of each support.
SA_{BET} is the specific area of the support in nm^2.
W_S is the weight of the support to impregnate.

$$N°Ni_{Imp} = \frac{N°OH_{av}}{2} \quad \text{Eq. F.2.}$$

Where,

$N°Ni_{Imp}$ is the number of the nickel atoms to impregnate.

$$W_{Ni}^{Max} = \frac{N°Ni_{Imp}}{NA} * AW_{Ni} \quad \text{Eq. F.3.}$$

Where,

W_{Ni}^{Max} is the Ni weight maximum to impregnate.
NA is the Avogadro number.
AW_{Ni} is the atomic weight of nickel.

$$w\%_{Ni}^{Max} = \frac{W_{Ni}^{Max}}{(W_{Ni}^{Max} + W_S)} \quad \text{Eq. F.4.}$$

Where,

$w\%_{Ni}^{Max}$ is the maximum impregnation weight percent of Ni to this support.

Since the silica is the support with the smallest specific area of all the supports studied, the calculation of maximum impregnation weight percent of Ni is based on this support, which is 0.5w%. This value was set for all synthesis.

Appendix G. Thermogravimetry analysis for the catalysts synthetized.

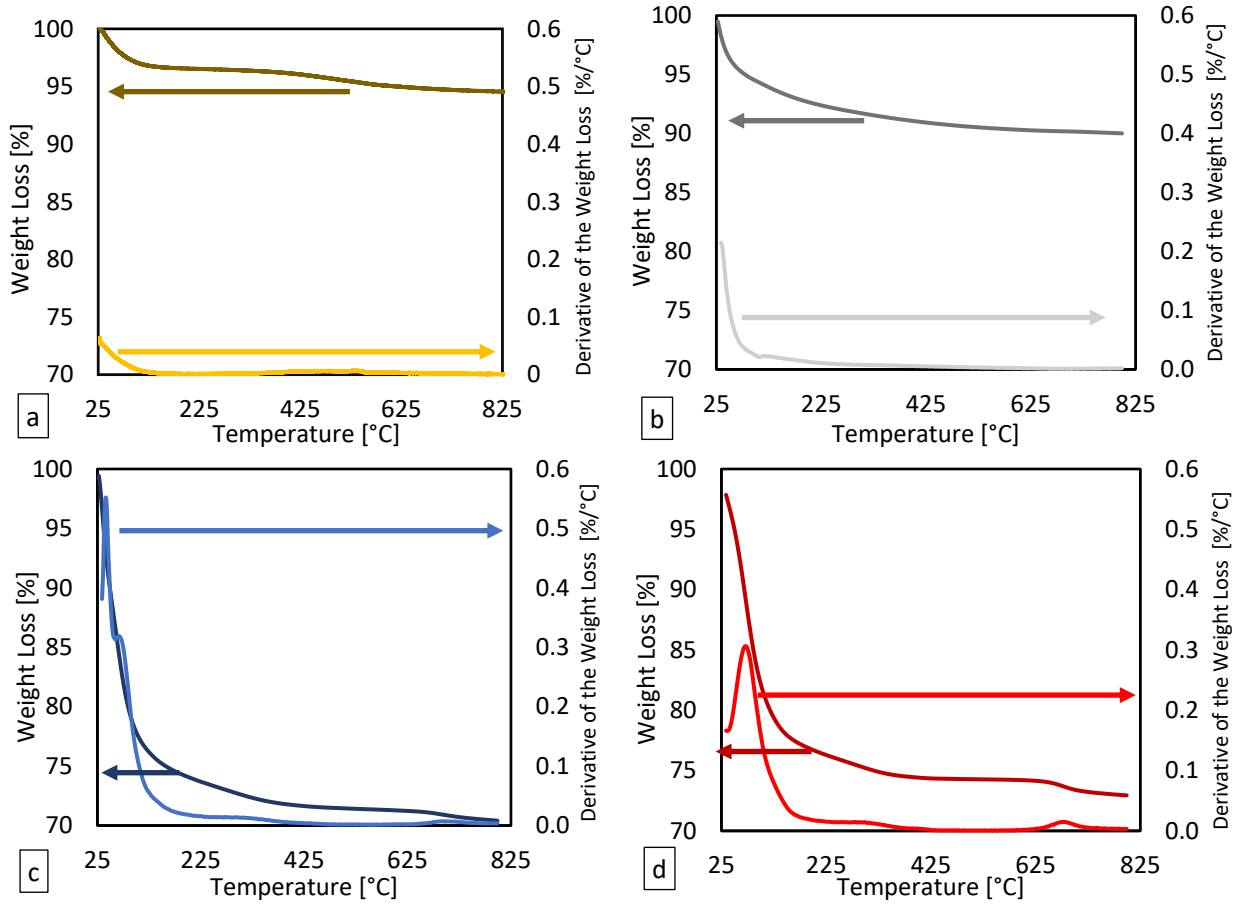

Figure G.1. TGA curves for the catalysts fresh (without calcinate). (a) Ni/SiO_2, (b) Ni/Al_2O_3, (c) Ni/HY, and, (d) Ni/HY-M.

Appendix H. Volume and size pore distribution for the catalysts.

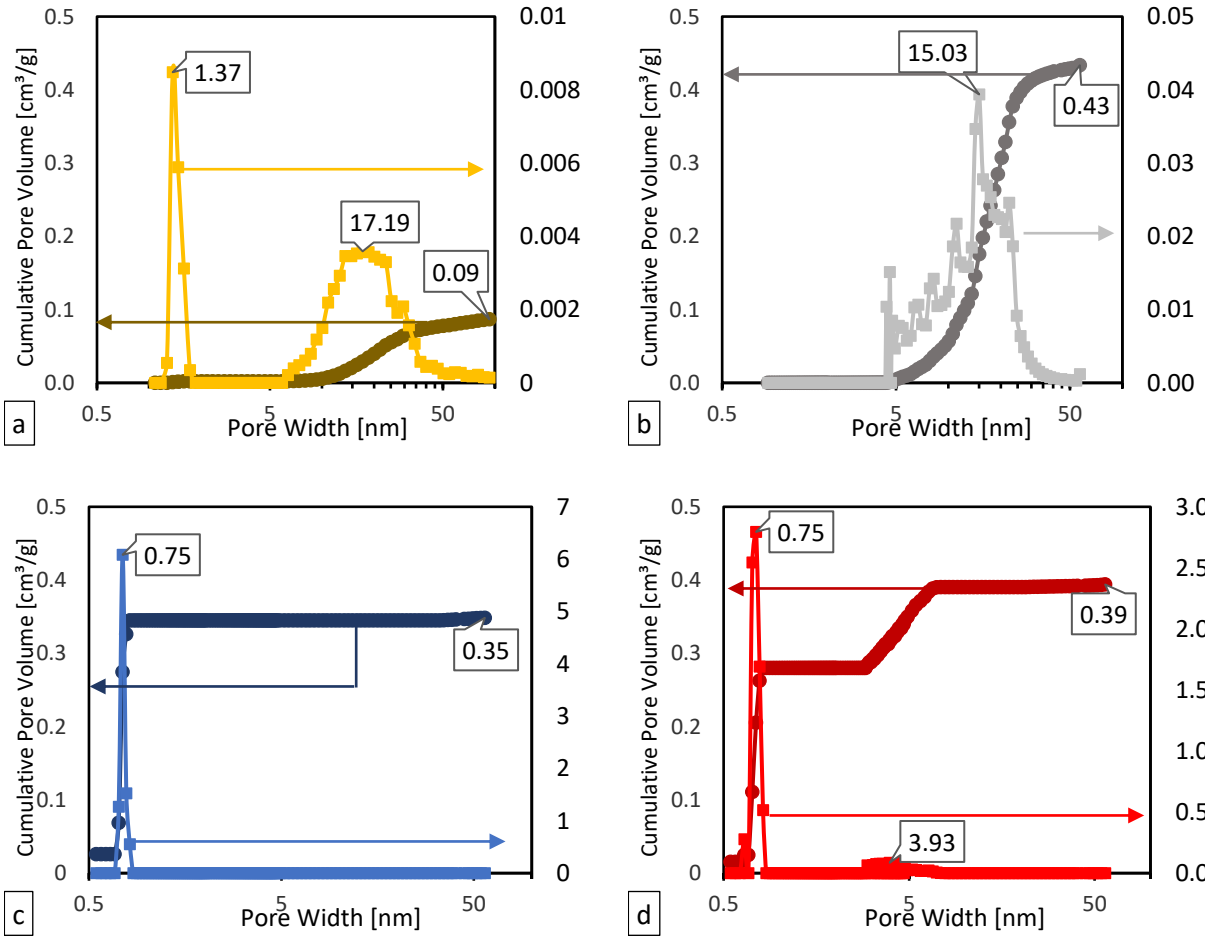

Figure H.1. Volume and size pore distribution for the powders of the catalysts using NLDFT method for (a) Ni/SiO_2, (b) Ni/Al_2O_3, (c) Ni/HY, and, (d) Ni/HY-M.

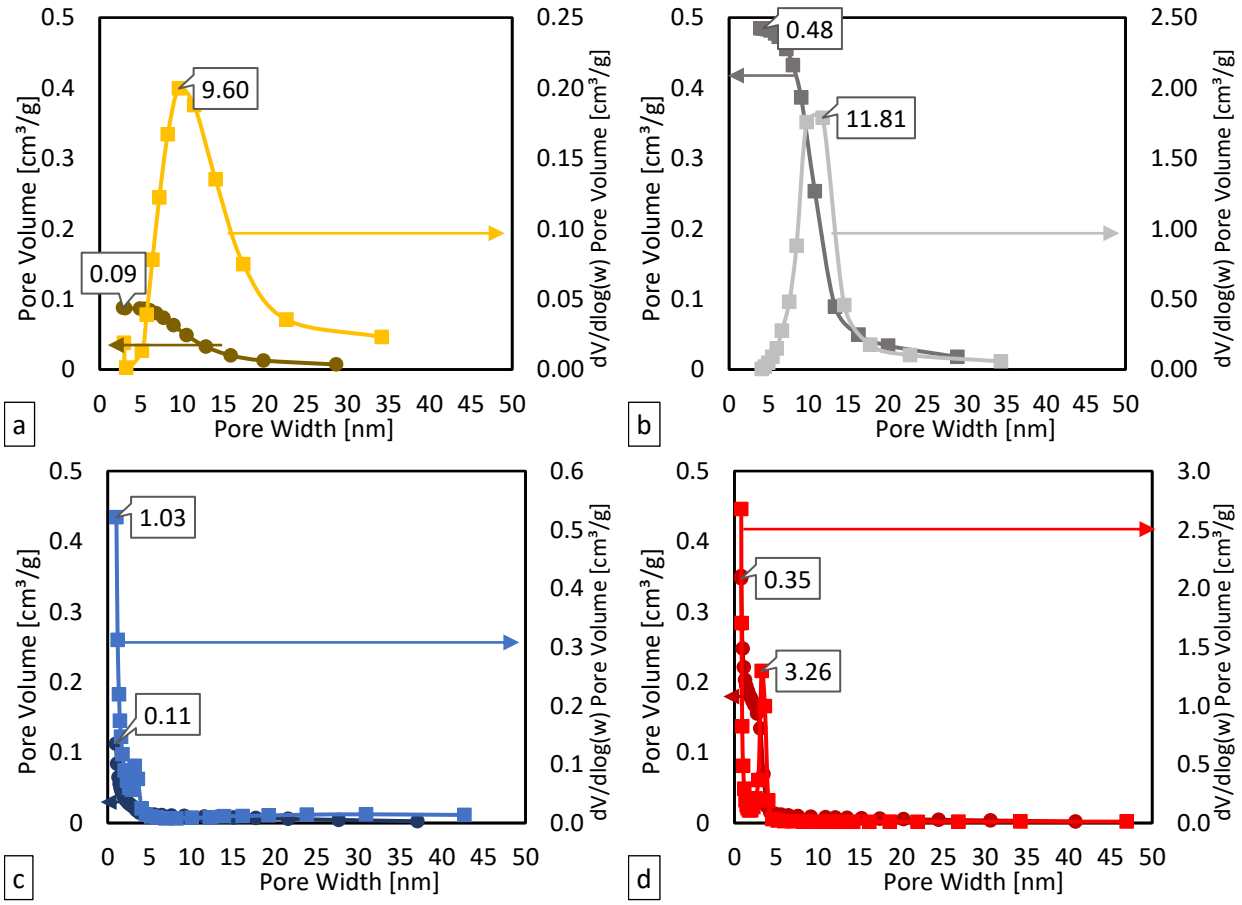

Figure H.2. Volume and size pore distribution for the powders of the catalysts using BJH method for (a) Ni/SiO_2, (b) Ni/Al_2O_3, (c) Ni/HY, and, (d) Ni/HY-M.

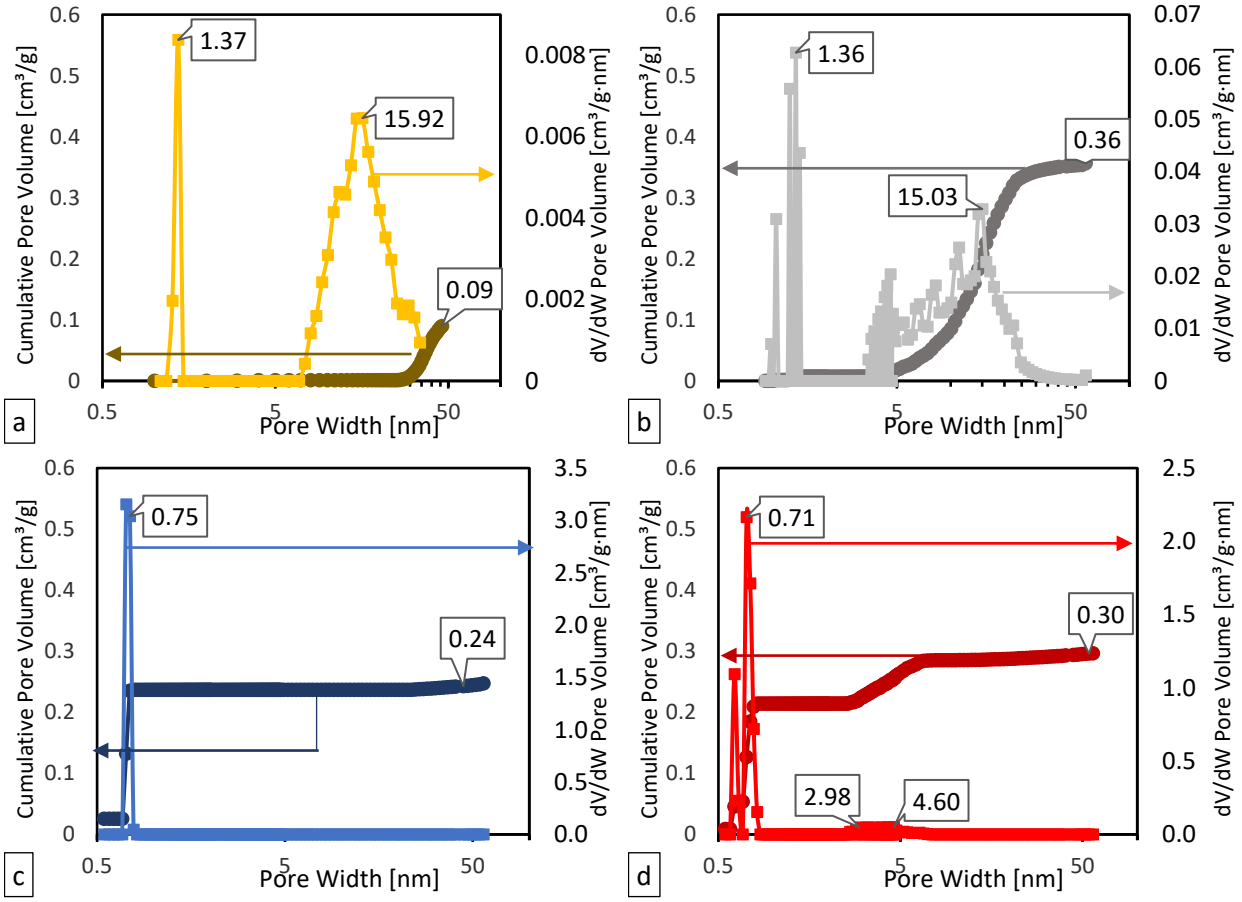

Figure H.3. Volume and size pore distribution for the catalysts pelletized, ground and sieved using NLDFT method for (a) Ni/SiO_2, (b) Ni/Al_2O_3, (c) Ni/HY, and, (d) Ni/HY-M.

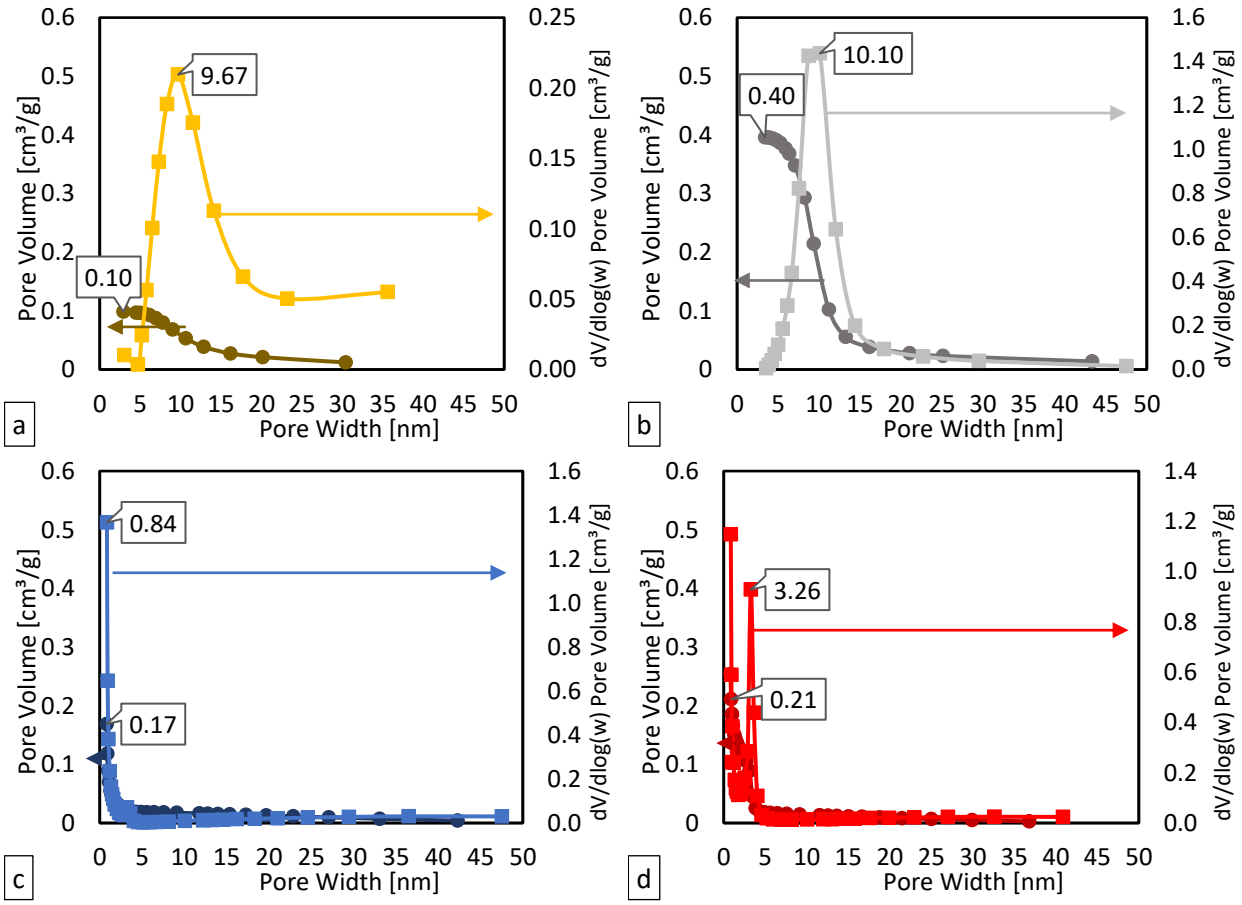

Figure H.4. Volume and size pore distribution for the catalysts pelletized, ground and sieved using BJH method for (a) Ni/SiO_2, (b) Ni/Al_2O_3, (c) Ni/HY, and, (d) Ni/HY-M.

Appendix I. Monitoring of the specific area and pore volume for each step in the synthesis of the catalysts.

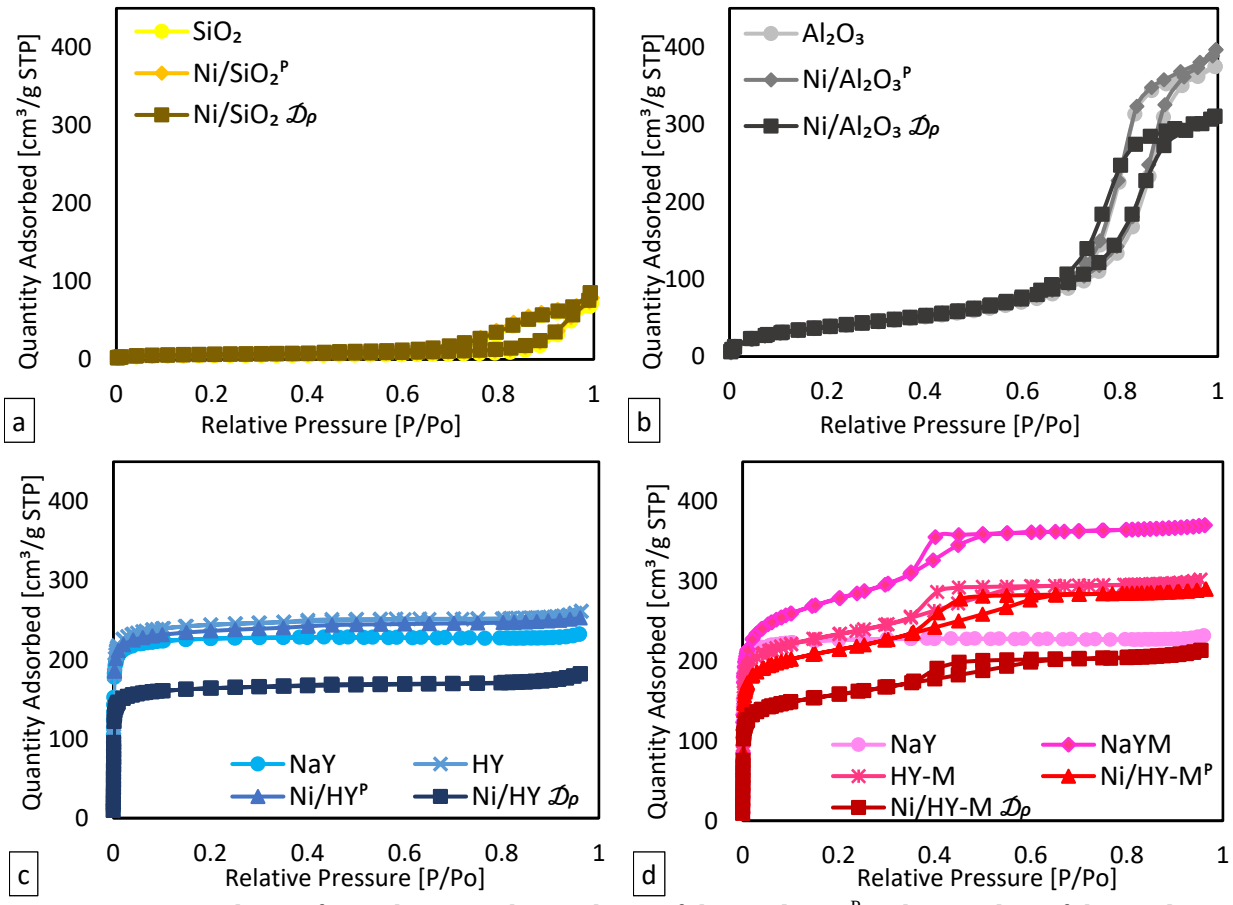

Figure I.1. Ar isotherms for each step in the synthesis of the catalysts. ^{P} is the powders of the catalyst, and, $\mathcal{D}_p$ is the catalyst pelletized, ground and sieved. For (a) SiO_2, (b) Al_2O_3, (c) HY, and, (d) HY-M. Measured at -186.15°C.

Table I.1.
Specific areas differences between each step in the synthesis of the catalysts. ^{P} is the powders of the catalyst, and, 𝒟𝓅 is the catalyst pelletized, ground and sieved.

Sample	SA_{BET} [$m^2 \cdot g^{-1}$]	Difference [%]	SA_{Micro} [$m^2 \cdot g^{-1}$]	Difference [%]	SA_{Meso} [$m^2 \cdot g^{-1}$]	Difference [%]
SiO_2	14	--	4	--	10	--
Ni/SiO_2^P	17	17	3	27	14	37
Ni/SiO_2 𝒟𝓅	19	15	4	24	15	13
Al_2O_3	128	--	--	--	136	--
$Ni/Al_2O_3^P$	130	2	--	--	148	9
Ni/Al_2O_3 𝒟𝓅	129	1	--	--	141	5
NaY	815	--	759	--	56	--
HY	870	7	788	4	83	48
Ni/HY^P	842	3	756	4	86	4
Ni/HY 𝒟𝓅	582	31	522	31	60	30
NaY	815	--	759	--	56	--
NaY-M	919	13	568	25	350	527
HY-M	789	14	557	2	231	34
$Ni/HY\text{-}M^P$	720	9	495	11	225	3
Ni/HY-M 𝒟𝓅	526	27	351	29	175	22

Table I.2.
Pore volumes differences between each step in the synthesis of the catalysts. ^{P} is the powders of the catalyst, and, 𝒟𝓅 is the catalyst pelletized, ground and sieved.

Sample	PV_{NLDFT} [$cm^3 \cdot g^{-1}$]	Difference [%]	PV_{BJH} [$cm^3 \cdot g^{-1}$]	Difference [%]
SiO_2	0.08	--	0.08	--
Ni/SiO_2^P	0.09	13	0.09	10
Ni/SiO_2 𝒟𝓅	0.09	3	0.10	12
Al_2O_3	0.44	--	0.48	--
$Ni/Al_2O_3^P$	0.43	1	0.48	2
Ni/Al_2O_3 𝒟𝓅	0.36	18	0.40	18
NaY	0.32	--	0.02	--
HY	0.36	12	0.12	510
Ni/HY^P	0.35	2	0.11	6
Ni/HY 𝒟𝓅	0.25	29	0.12	5
NaY	0.32	--	0.02	--
NaY-M	0.51	60	0.25	1159
HY-M	0.42	18	0.37	48
$Ni/HY\text{-}M^P$	0.39	6	0.35	4
Ni/HY-M 𝒟𝓅	0.30	25	0.25	28

Appendix J. Determination of the OH sites concentration for the catalysts.

Appendix J.1. For the Ni/Al_2O_3.

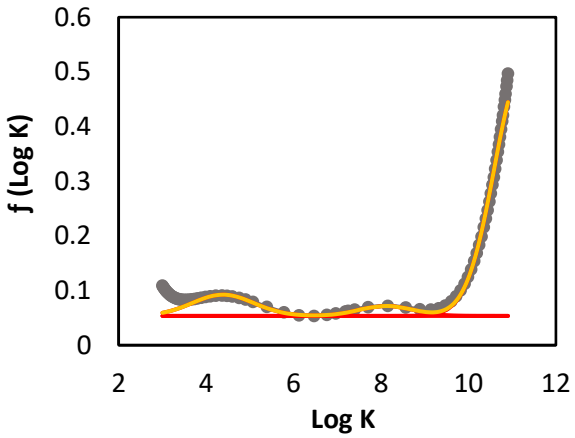

Figure J.1.1. Proton affinity distribution as a function of pH for Ni/Al_2O_3 and peak decomposition.

Table J.1.1.
Quantification of the concentration of OH groups depending of the type of site for Al_2O_3.

Catalyst	C [$mmolH^+ \bullet g^{-1}$ of support]		
	IIA	IA	IB
Ni/Al_2O_3	0.069	0.028	0.712

Appendix J.2. For the Ni/SiO_2.

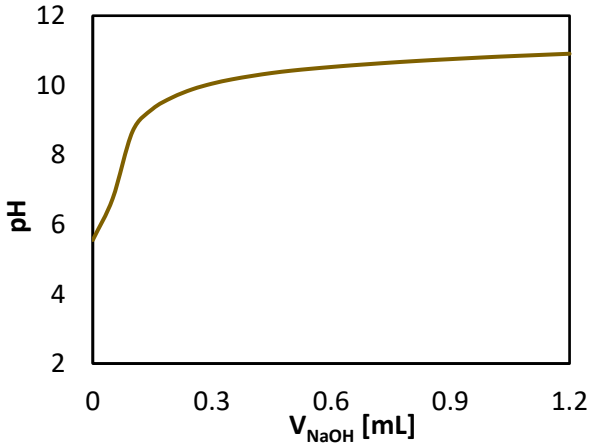

Figure J.2.1. Titration of Ni/SiO_2 using a strong base (NaOH) in order to calculate the concentration of silanol groups.

Appendix J.3. For Ni/HY, Ni/HY-M, and, Ni/HY-M*.

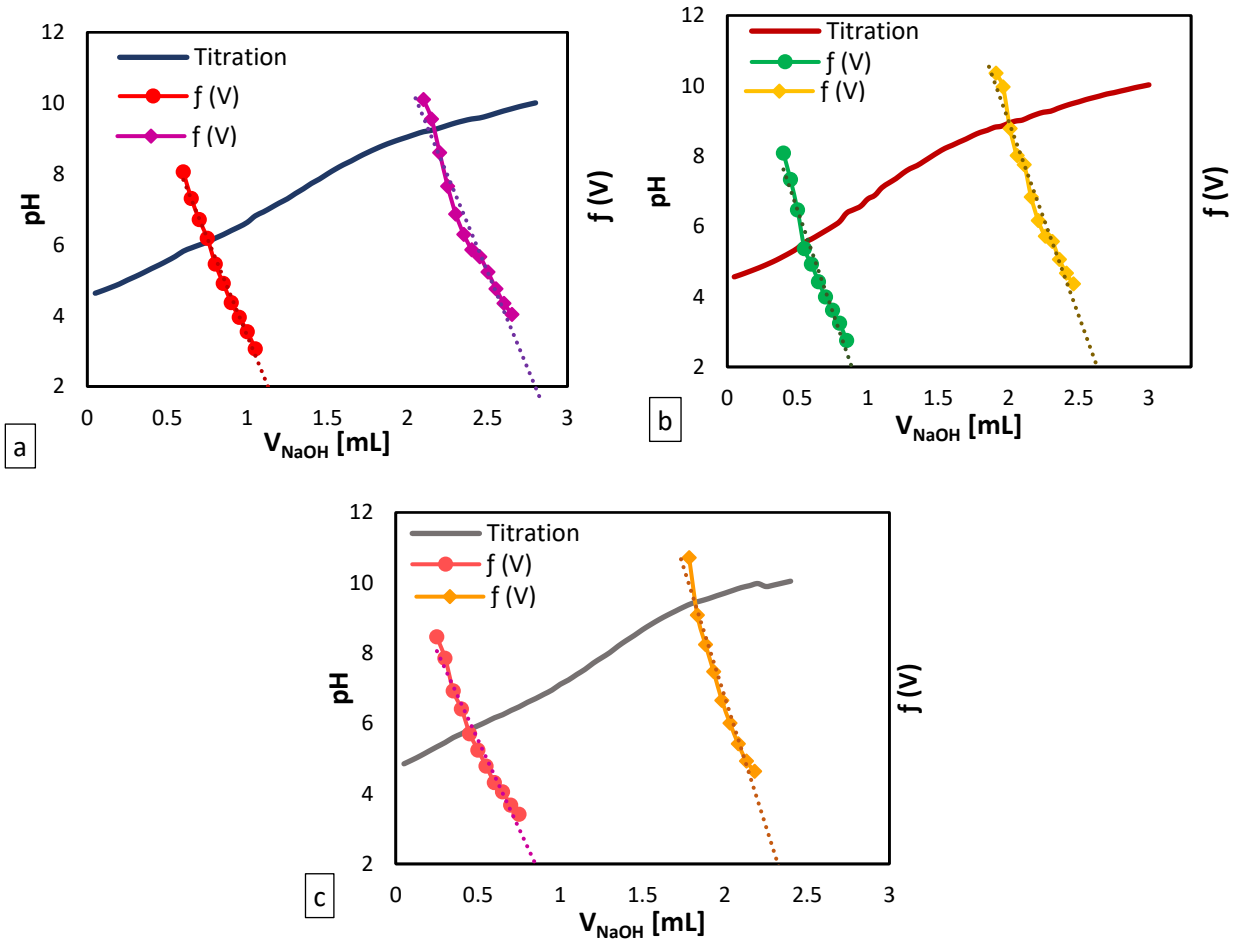

Figure J.3.1. Determination of the acid sites with the Gran method in titration of (a) Ni/HY zeolite, (b) HY-M zeolite, and (c) Ni/HY-M* (from incipient wetness impregnation method). The points marked with circles (reds, greens, and pink) and diamonds (purples, yellows, and orange) are obtained by transforming the original titration data with the Gran f(V) (Eq. E.3.8.). The numerical scales for the different functions of f(V) are not shown.

Table J.3.1.
Quantification of the concentration of acid sites for Ni/HY, Ni/HY-M, and, Ni/HY-M.*

Support	C [mmolH^+•g^{-1} of support]	
	$R_1^- H^+$	$R_2^- H^+$
Ni/HY	0.500	0.745
Ni/HY-M	0.500	0.750
Ni/HY-M*	0.501	1.002

Appendix K. Conditions to carry out the catalytic tests.

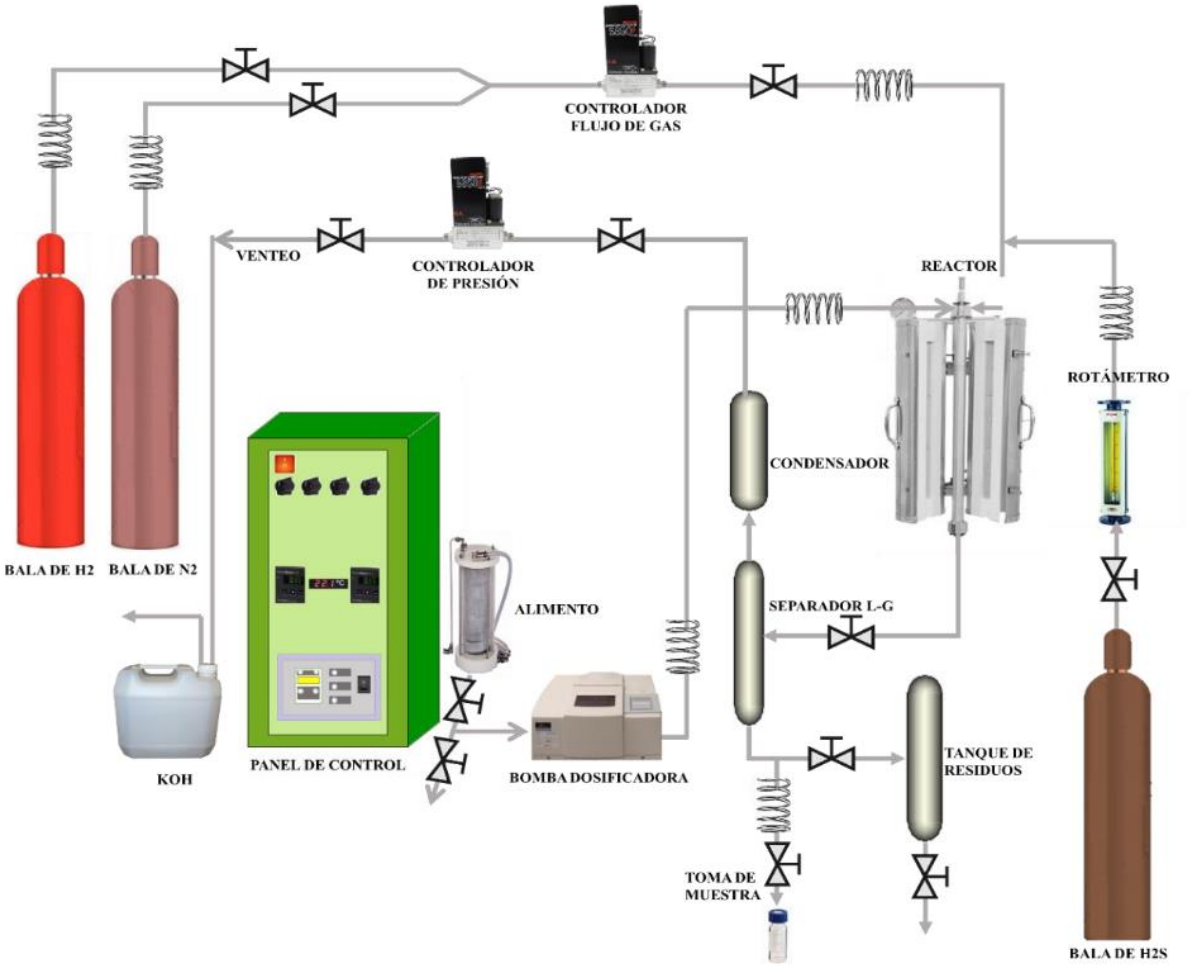

Figure K.1. Scheme of the reaction system. Taken of (Santiago Guerrero & Elder Bueno, 2019).

Taking into account that for all reactions the concentration of DBT was maintained at 2.2%, and according to conventional HDS reactions using a commercial catalyst with 1.8w% Ni (Morales-Valencia, Castillo-Ariza, Giraldo, & Baldovino-Medrano, 2018; Morales-Valencia E. M., 2019), the necessary mass of catalyst was calculated to carry out each reaction, and its shows in Table K.1.

Table K.1.
Quantity of catalyst to reactions.

	Commercial Catalyst	**This Work**
Ni wt%	1.8	0.5
Catalyst Weight [g]	0.15	0.54
Ni Weight [g]	$2.7x10^{-3}$	$2.7x10^{-3}$

Appendix L. Reactions schemes and active sites supposed.

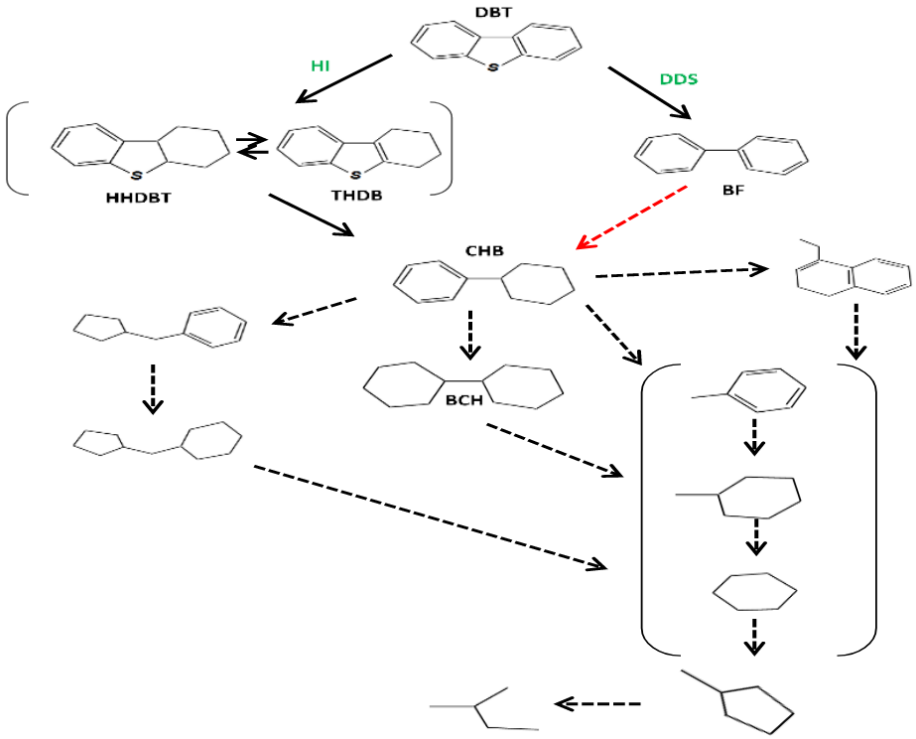

Figure L.1. Reaction scheme in the HDS of DBT with molecules cracking proposed by Ojeda and Rincón. Taken of (Ojeda-Niño & Rincón-Ortiz, 2014).

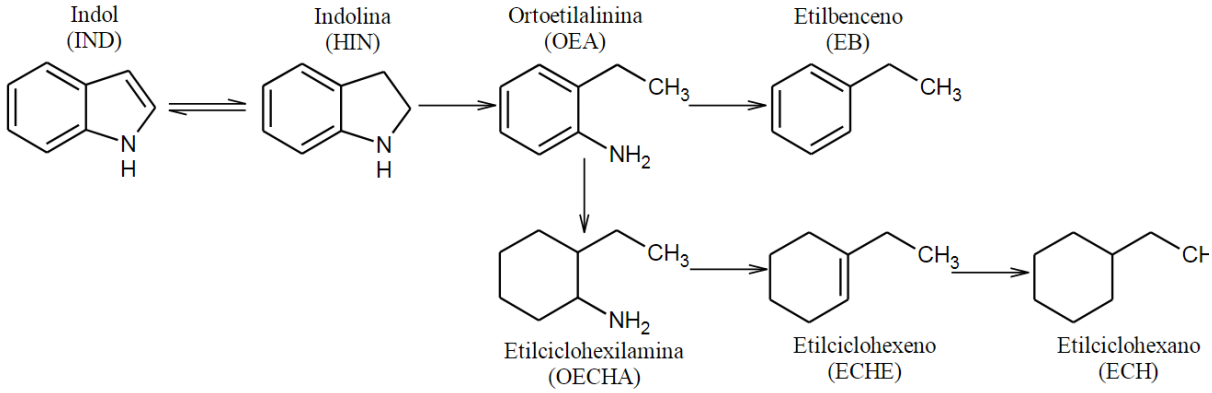

Figure L.2. Reaction scheme in the HDN of indole. Taken of (Laredo & Altamirano, 2003).

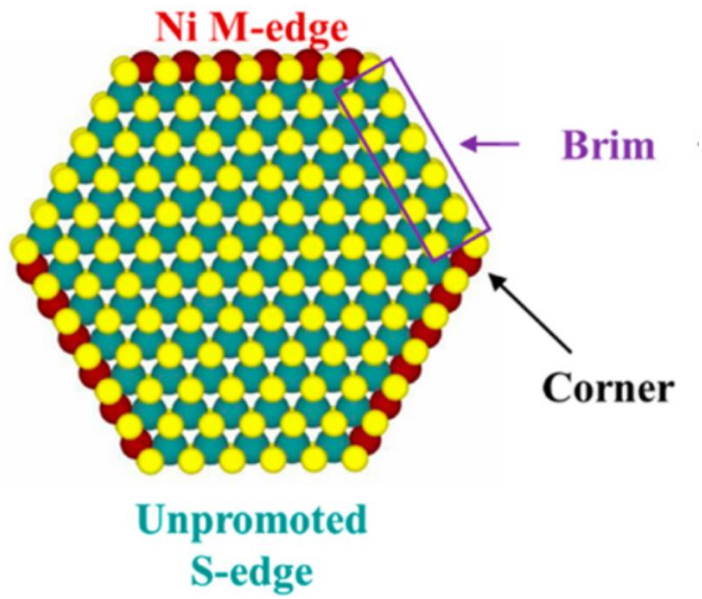

Figure L.3. Active sites supposed of a commercial catalyst. A representative particle model of NiMoS with Ni atoms replacing Mo atoms on the metal edge. The three types of sites (edge, corner, and brim) are marked for reference. Color scheme: violet, cobalt; red, nickel; cyan, molybdenum; yellow, sulfur. Taken of (Rangarajan & Mavrikakis, 2017).

Appendix M. Identification of some of the products of DBT conversion.

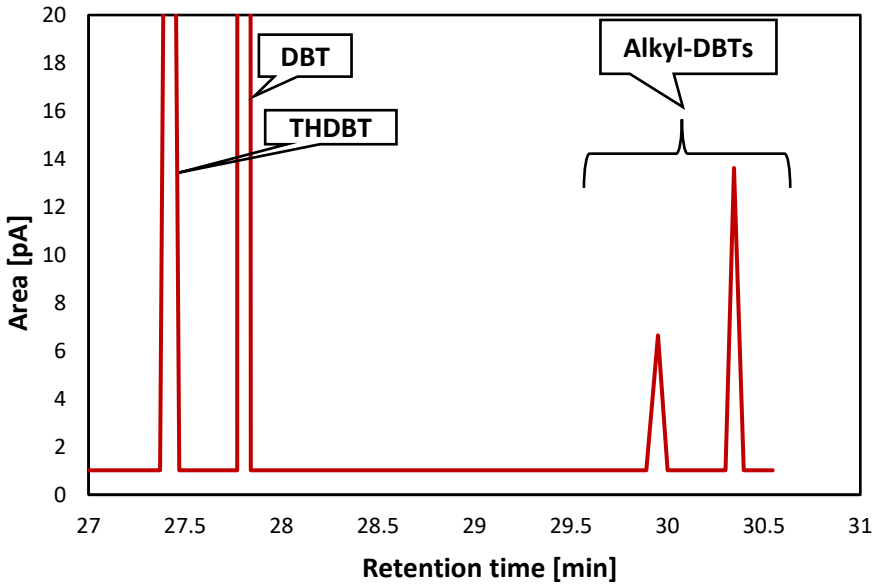

Figure M. Chromatogram of HDS of DBT over Ni/HY-M for some of the DBT products.

Appendix N. Carbon balance for HDT reactions using Ni/SiO_2, Ni/Al_2O_3, Ni/HY, Ni/HY-M, and Ni/HY-M* catalysts.

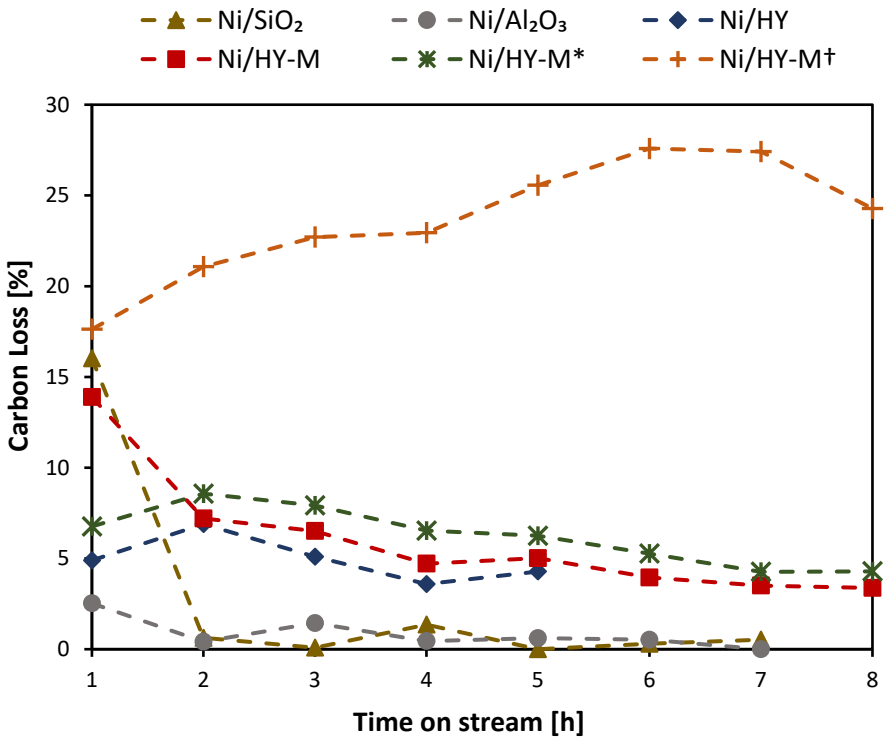

Figure N. Carbon Loss in the HDT reactions. *From the incipient wetness impregnation method. †HDS of DBT in presence of indole.